


An Assessment of CO₂ Uptake in the Arctic Ocean From 1985 to 2018

Journal Article**Author(s):**

Yasunaka, Sayaka; Manizza, Manfredi; Terhaar, Jens; Olsen, Are; Yamaguchi, Ryohei; Landschützer, Peter; Watanabe, Eiji; Carroll, Dustin; Adiwira, Hanani; [Müller, Jens Daniel](#) ; Hauck, Judith

Publication date:

2023-11

Permanent link:

<https://doi.org/10.3929/ethz-b-000642560>

Rights / license:

[Creative Commons Attribution-NonCommercial 4.0 International](#)

Originally published in:

Global Biogeochemical Cycles 37(11), <https://doi.org/10.1029/2023GB007806>

Funding acknowledgement:

821003 - Climate-Carbon Interactions in the Coming Century (EC)

Global Biogeochemical Cycles®



RESEARCH ARTICLE

10.1029/2023GB007806

An Assessment of CO₂ Uptake in the Arctic Ocean From 1985 to 2018

Special Section:

Regional Carbon Cycle Assessment and Processes - 2

Sayaka Yasunaka^{1,2} , Manfredi Manizza³ , Jens Terhaar^{4,5,6} , Are Olsen⁷ , Ryohei Yamaguchi² , Peter Landschützer^{8,9} , Eiji Watanabe² , Dustin Carroll¹⁰ , Hanani Adiwira¹ , Jens Daniel Müller¹¹ , and Judith Hauck¹² 

Key Points:

- The Arctic Ocean is estimated to be a net sink of CO₂ of 116 ± 4 TgC yr⁻¹ in *p*CO₂ products and 92 ± 30 TgC yr⁻¹ in ocean models
- The Arctic Ocean CO₂ uptake is explained by a steady-state natural flux (70%) with atmospheric CO₂ increase (19%) and climate change (11%)
- The CO₂ uptake increased (31 ± 13 TgC yr⁻¹ dec⁻¹ in products and 10 ± 4 TgC yr⁻¹ dec⁻¹ in models) mostly by decreasing sea ice

Supporting Information:

Supporting Information may be found in the online version of this article.

Correspondence to:

S. Yasunaka,
yasunaka@tohoku.ac.jp

Citation:

Yasunaka, S., Manizza, M., Terhaar, J., Olsen, A., Yamaguchi, R., Landschützer, P., et al. (2023). An assessment of CO₂ uptake in the Arctic Ocean from 1985 to 2018. *Global Biogeochemical Cycles*, 37, e2023GB007806. <https://doi.org/10.1029/2023GB007806>

Received 15 APR 2023

Accepted 9 OCT 2023

Author Contributions:

Conceptualization: Sayaka Yasunaka, Manfredi Manizza, Jens Terhaar
Data curation: Sayaka Yasunaka, Jens Daniel Müller
Formal analysis: Sayaka Yasunaka, Ryohei Yamaguchi
Funding acquisition: Sayaka Yasunaka

¹Graduate School of Science, Tohoku University, Sendai, Japan, ²Japan Agency for Marine-Earth Science and Technology, Yokosuka, Japan, ³Geosciences Research Division, Scripps Institution of Oceanography, University of California, San Diego, La Jolla, CA, USA, ⁴Department of Marine Chemistry and Geochemistry, Woods Hole Oceanographic Institution, Woods Hole, MA, USA, ⁵Physics Institute, University of Bern, Bern, Switzerland, ⁶Oeschger Centre for Climate Change Research, University of Bern, Bern, Switzerland, ⁷Bjerknes Centre for Climate Research, Geophysical Institute, University of Bergen, Bergen, Norway, ⁸Flanders Marine Institute (VLIZ), Ostend, Belgium, ⁹Max Planck Institute for Meteorology, Hamburg, Germany, ¹⁰Moss Landing Marine Laboratories, San José State University, San Jose, CA, USA, ¹¹Environmental Physics, Institute of Biogeochemistry and Pollutant Dynamics, ETH Zurich, Zürich, Switzerland, ¹²Alfred Wegener Institute for Polar and Marine Research, Bremerhaven, Germany

Abstract As a contribution to the Regional Carbon Cycle Assessment and Processes phase 2 (RECCAP2) project, we present synthesized estimates of Arctic Ocean sea-air CO₂ fluxes and their uncertainties from surface ocean *p*CO₂-observation products, ocean biogeochemical hindcast and data assimilation models, and atmospheric inversions. For the period of 1985–2018, the Arctic Ocean was a net sink of CO₂ of 116 ± 4 TgC yr⁻¹ in the *p*CO₂ products, 92 ± 30 TgC yr⁻¹ in the models, and 91 ± 21 TgC yr⁻¹ in the atmospheric inversions. The CO₂ uptake peaks in late summer and early autumn, and is low in winter when sea ice inhibits sea-air fluxes. The long-term mean CO₂ uptake in the Arctic Ocean is primarily caused by steady-state fluxes of natural carbon ($70\% \pm 15\%$), and enhanced by the atmospheric CO₂ increase ($19\% \pm 5\%$) and climate change ($11\% \pm 18\%$). The annual mean CO₂ uptake increased from 1985 to 2018 at a rate of 31 ± 13 TgC yr⁻¹ dec⁻¹ in the *p*CO₂ products, 10 ± 4 TgC yr⁻¹ dec⁻¹ in the models, and 32 ± 16 TgC yr⁻¹ dec⁻¹ in the atmospheric inversions. Moreover, $77\% \pm 38\%$ of the trend in the net CO₂ uptake over time is caused by climate change, primarily due to rapid sea ice loss in recent years. Furthermore, true uncertainties may be larger than the given ensemble standard deviations due to common structural biases across all individual estimates.

Plain Language Summary The Arctic Ocean is at present a net sink for atmospheric CO₂ mainly due to the intense cooling of the inflowing waters from the Atlantic and the Pacific. Global warming is amplified in the Arctic Ocean and it experiences a rapid retreat of sea ice. Here, we present synthesized estimates of the Arctic Ocean CO₂ uptake and their uncertainties from estimates obtained using different methods. Almost all estimates suggest that the Arctic Ocean was a net sink of CO₂ from 1985 to 2018. The CO₂ uptake is strong in late summer and early autumn and weak in winter, corresponding to the seasonal variation of sea ice. CO₂ uptake has increased in recent years, especially in regions that have experienced sea ice loss. Compared to the global ocean, the Arctic Ocean is unique because climate change, in particular the change in sea ice cover, has enhanced the ocean CO₂ uptake almost as much as the increase in atmospheric CO₂ over the past 34 years. Moreover, this climate effect on the Arctic Ocean CO₂ uptake has become more important in recent years and is the current main driver for the trend toward an increasing CO₂ uptake in the Arctic Ocean.

1. Introduction

The Arctic Ocean, which consists of complex subregions that include continental shelves and a central basin (Figure 1), has previously been estimated to represent a sink for atmospheric CO₂ (Bates & Mathis, 2009; Manizza et al., 2013, 2019; Yasunaka et al., 2018). The rapid cooling of the inflowing Atlantic and Pacific waters through the Barents Sea and the Chukchi Sea (Vowinkel & Orvig, 1962) increases the solubility of CO₂ (Weiss, 1974) and hence allows these waters to take up CO₂ from the atmosphere (Anderson & Kaltin, 2001). The sea-air CO₂ flux is mainly modulated by the surface ocean partial pressure of CO₂ (*p*CO_{2,w}), the wind speed, and the sea ice cover

© 2023 The Authors.

This is an open access article under the terms of the [Creative Commons Attribution-NonCommercial License](#), which permits use, distribution and reproduction in any medium, provided the original work is properly cited and is not used for commercial purposes.

Investigation: Sayaka Yasunaka, Manfredi Manizza, Peter Landschützer, Eiji Watanabe, Dustin Carroll
Methodology: Sayaka Yasunaka, Manfredi Manizza, Are Olsen
Software: Sayaka Yasunaka
Supervision: Jens Daniel Müller, Judith Hauck
Visualization: Sayaka Yasunaka
Writing – original draft: Sayaka Yasunaka, Manfredi Manizza, Jens Terhaar, Are Olsen
Writing – review & editing: Sayaka Yasunaka, Manfredi Manizza, Jens Terhaar, Are Olsen, Ryohei Yamaguchi, Peter Landschützer, Eiji Watanabe, Dustin Carroll, Jens Daniel Müller, Judith Hauck

that acts as a barrier for the exchange of gasses across the sea-air interface (Bates & Mathis, 2009). While sea ice cover and wind speed are relatively well known from satellite missions and reanalysis products (e.g., Comiso et al., 2008; Hersbach et al., 2020), large uncertainties in $p\text{CO}_{2w}$ remain and make it challenging to quantify both the direction and magnitude of the sea-air CO_2 exchange (Yasunaka et al., 2018). In the Arctic Ocean, $p\text{CO}_{2w}$ is influenced by many factors, such as ocean heat loss and gain, the influx of Atlantic and Pacific water masses, biological production and respiration, sea ice formation and melting, river discharge, land-ocean carbon fluxes from rivers and coastal erosion, vertical mixing, and shelf–basin interactions (Anderson et al., 2009; Bates, 2006; Bates & Mathis, 2009; Fransson et al., 2017; Kaltin & Anderson, 2005; Manizza et al., 2011; Olsen et al., 2015; Oziel et al., 2022; Terhaar, Orr, Ethé, et al., 2019; Terhaar, Orr, Gehlen, et al., 2019). The combination of these environmental drivers results in large spatiotemporal variations in Arctic Ocean CO_2 uptake.

As global warming progresses and sea ice further retreats (Notz & Stroeve, 2016), sea-air CO_2 fluxes in the Arctic Ocean might become more important over the 21st century. In recent decades, Arctic surface air temperatures have been increasing at least twice as fast as globally averaged surface air temperatures (Meredith et al., 2019; Rantanen et al., 2022). This is known as “Arctic Amplification” (Screen & Simmonds, 2010) and results in rapid sea ice decline. Melting of sea ice increases the open water area and thus enhances the potential for atmospheric CO_2 uptake (e.g., Anderson & Kaltin, 2001; Bates et al., 2006; Gao et al., 2012; Qi et al., 2022). CO_2 uptake might also be increased by enhanced primary production in the Arctic Ocean due to more light availability at the ocean surface (Arrigo & van Dijken, 2015) and increased nutrient delivery from rivers and coastal erosion (Frey & McClelland, 2009; Terhaar, Orr, Ethé, et al., 2019). However, other processes may suppress the CO_2 uptake. For example, increasing seawater temperatures, declining buffer capacity due to the freshening of Arctic Ocean surface water by increased river runoff and melting of sea ice, increased vertical mixing supplying high- CO_2 water to the surface, and increased carbon fluxes from rivers and coastal erosions (Bates & Mathis, 2009; Bates et al., 2014; Cai et al., 2010; Chierici et al., 2011; Else et al., 2013; Fransson et al., 2017; Hauri et al., 2013; McGuire et al., 2010; Nielsen et al., 2022; Tank et al., 2016; Terhaar, Orr, Ethé, et al., 2019). Furthermore, an increased inflow of Atlantic water (Oziel et al., 2020; Wang et al., 2020) that is rich in anthropogenic carbon (MacGilchrist et al., 2014; Terhaar, Orr, Gehlen, et al., 2019) will likely further decrease the CO_2 uptake and can even result in the outgassing of anthropogenic CO_2 (Anderson & Olsen, 2002; Terhaar, Tanhua, et al., 2020; Völker et al., 2002). At the end of the 21st century, Earth System Models predict a reversal of the $p\text{CO}_{2w}$ seasonality in Arctic Ocean surface waters (Orr et al., 2022), with so far unknown consequences for the functioning of the Arctic Ocean CO_2 sink.

For the assessment of changes in $p\text{CO}_{2w}$ and sea-air CO_2 flux, including their regional and seasonal patterns, it is crucial to establish a baseline against which changes can be evaluated. However, establishing such a baseline in the Arctic Ocean is complicated due to sparse observations in this hostile and remote ocean basin, especially in the sea ice covered regions and periods (Yasunaka et al., 2016). As a result, the current uncertainty of Arctic Ocean CO_2 flux estimates is large, despite the use of various statistical techniques and numerical models (Bates & Mathis, 2009; Yasunaka et al., 2018). Bates and Mathis (2009) summarized regional CO_2 flux estimates from the Arctic Ocean and arrived at a net sink strength of between 66 and 199 Tg C yr^{-1} . In addition, the first implementation of the Regional Carbon Cycle Assessment and Processes project (RECCAP) also assessed the Arctic Ocean CO_2 fluxes but treated the Arctic Ocean as one part of the “large-scale Atlantic Ocean basin” north of 44°S (Schuster et al., 2013). In the first implementation of RECCAP, a small Arctic Ocean CO_2 sink of $50 \pm 30 \text{ Tg C yr}^{-1}$ was estimated from available observational $p\text{CO}_{2w}$ -based estimates, ocean biogeochemical model outputs and atmospheric inversions. However, it was concluded that one could not reliably constrain the Arctic Ocean CO_2 uptake because of limited data and poorly resolved processes in the physical and/or biogeochemical models. Since that assessment, the number of available $p\text{CO}_{2w}$ measurements have continuously increased (>60% of available $p\text{CO}_{2w}$ data in the Arctic Ocean have been collected after 2010; Figure S1 in Supporting Information S1), and ocean biogeochemical models have improved in terms of spatial resolution and additional processes such as eddy transport (Chassignet et al., 2020), sea ice ecosystem (Watanabe et al., 2019), and riverine nutrient and carbon input (e.g., Séférian et al., 2019) in some models.

Here we build on these recent developments and present an updated assessment of the Arctic Ocean CO_2 uptake as part of the RECCAP phase 2 (RECCAP2) project. In this dedicated Arctic Ocean chapter, we integrate and assess recent results from $p\text{CO}_2$ products based on $p\text{CO}_{2w}$ observations, from ocean biogeochemical hindcast and data assimilation models and from atmospheric inversions, and present synthesized estimates of the Arctic Ocean

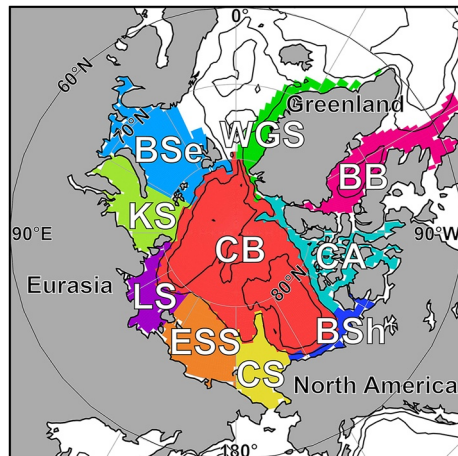


Figure 1. Regional masks in the Arctic Ocean: Central Basin (CB), western Greenland Sea (WGS), Baffin Bay (BB), Canadian Archipelago (CA), Beaufort Shelf (BSh), Chukchi Sea (CS), East Siberian Sea (ESS), Laptev Sea (LS), Kara Sea (KS), Barents Sea (BSe). Contour lines show 1,000 and 3,000 m isobaths.

CO₂ uptake together with its drivers and uncertainties. We also examine CO₂ fluxes in the various subregions of the Arctic Ocean and their seasonal and interannual variations.

2. Data and Methods

2.1. Regional Mask

The Arctic Ocean is here defined by the RECCAP2 regional mask (Figure 1). The outer boundary follows Fay and McKinley (2014), which defined the Arctic Ocean as the ocean having more than 50% sea ice concentration (SIC) in the period 1998–2010, with some modifications: the boundary between the Arctic Ocean and the North Atlantic extends to 56°N in the Labrador Sea, while at 25°E it is located at the northern tip of the Scandinavian peninsula. The boundary between the Arctic Ocean and the North Pacific is set to the Bering Strait following the World Ocean Atlas 2009 (Levitus, 2013).

The Arctic Ocean is further divided into 10 subregions: the Central Basin, the western Greenland Sea, the Baffin Bay (including the western Labrador Sea), the Canadian Archipelago, the Beaufort Shelf, the Chukchi Sea, the East Siberian Sea, the Laptev Sea, the Kara Sea, and the Barents Sea (Figure 1). The boundary between the Central Basin and the surrounding marginal shelf seas is defined by the 1,000 m isobath. The RECCAP2 mask here is different

from the mask that was used by Bates and Mathis (2009) and in the first phase of RECCAP (Schuster et al., 2013); neither of these included the Baffin Bay and the western Greenland Sea in the Arctic Ocean.

2.2. Sea-Air CO₂ Flux and pCO_{2w} Estimates

The estimates of the sea-air CO₂ flux and pCO_{2w} in the Arctic Ocean used in this study were obtained from 8 pCO₂ products based on pCO_{2w} observations, 18 ocean biogeochemical hindcast and data assimilation models, and 6 atmospheric inversions (Table 1). Among them, 23 data sets belong to the RECCAP2 data compilation (see DeVries et al., 2023 for detail). All RECCAP2 data sets that cover the Arctic Ocean were used. FESOM_RECoM_HR, which was not included in the global chapter, was used in addition to FESOM_RECoM_LR here because its high spatial resolution allows better representation of the carbon dynamics in the marginal shelf seas and of the horizontal transport in and out of the Arctic Ocean (Chassignet et al., 2020). Another four data sets were used exclusively in the Arctic chapter of RECCAP2: Arctic-SOM, SOM-FFN-extended, Arctic_NEMURO-C, and ECCO2-Darwin. Arctic-SOM is an observational pCO₂ based product for the Arctic Ocean calculated using the self-organizing map technique by Yasunaka et al. (2018) extended until 2017. SOM-FFN-extended is an updated pCO₂ product including the Arctic Ocean, in contrast to the standard SOM-FFN that is part of RECCAP2 data compilation. The largest difference from the standard SOM-FFN is, besides the inclusion of the Arctic domain, the use of a different mixed layer depth product (MIMOC, Schmidt et al., 2013) as part of the explaining parameters. These changes are documented in Landschützer et al. (2020). Arctic_NEMURO-C is an ocean biogeochemical model including sea ice ecosystem component, coupled with the pan-Arctic sea ice-ocean model COCO (Watanabe et al., 2019). ECCO2-Darwin is an ocean biogeochemical model with the assimilation of physical data, which simulates the global ocean but with the main focus in the Arctic Ocean (Manizza et al., 2019). Since CAMS and Jena-CarboScope in the RECCAP2 compilation were archived after 1990, it is downloaded from the original sites.

The pCO₂ products are based on observed pCO_{2w} values, and fill temporal and spatial gaps in the observations using various techniques (e.g., multiple regressions and machine learning). The models are forced with historical time-evolving atmospheric pCO₂ (pCO_{2a}) and climate conditions (such as atmospheric temperature, humidity and wind fields; Simulation (Sim) A). In addition to the global and regional ocean biogeochemical hindcast models, ocean data assimilation models that assimilate observed distributions of temperature, salinity, and other physical and/or chemical parameters are used. Since there is no large difference in CO₂ flux and pCO_{2w} between the hindcast models and the data assimilation models (see Figures S2 and S3 in Supporting Information S1), they are treated as a single category. Potential model drift in the sea-air CO₂ flux was assessed as the slope of

Table 1
CO₂ Flux and pCO_{2w} Estimates Used in This Study

Name	Version	Period	Notes	Reference
pCO₂ products				
AOML-EXTRAT	v20211130	1997–2020	No data in sea ice region	Pierrot et al. (2009)
CMEMS-FFNN	v20210709	1985–2018	No data in sea ice region	Chau et al. (2022)
Jena-MLS ^a	v20211126	1985–2018		Rödenbeck et al. (2022)
NIES-ML3	v20220222	1985–2021	No data in sea ice region	Zeng et al. (2022)
OceanSODAETHZ ^a	v20211207	1985–2018		Gregor and Gruber (2021)
Takahashi-climatology	v20210702	–	Climatology; No data in sea ice region	Takahashi et al. (2009)
Arctic-SOM	v202301	1997–2017	Arctic only	Yasunaka et al. (2018)
SOM-FFN-extended ^a	v32	1983–2019		Landschützer et al. (2020)
Ocean biogeochemical hindcast and data assimilation models				
CCSM-WHOI ^b	v20211125	1958–2017	No riverine carbon flux	Doney et al. (2009)
CESM-ETHZ ^{a,b}	v20211122	1980–2018		Yang and Gruber (2016)
CNRM-ESM2 ^{a,b}	v20211208	1980–2018		Séférian et al. (2019)
EC-Earth3 ^{a,b}	v20210726	1980–2018		Döscher et al. (2022)
ECCO-Darwin	v20210712	1995–2018	Data assimilation; No riverine carbon flux	Carroll et al. (2020)
FESOM_REcoM_HR ^a	v20211119	1980–2018	No riverine carbon flux	Hauck et al. (2020)
FESOM_REcoM_LR ^{a,b}	v20211119	1980–2018	No riverine carbon flux	Hauck et al. (2020)
MOM6-Princeton ^a	v20220125	1980–2018		Stock et al. (2020)
MPIOM-HAMOCC ^{a,b}	20220110	1980–2019	No riverine carbon flux	Mauritsen et al. (2019)
MRI-ESM2 ^{a,b}	v20220502	1980–2018	No riverine carbon flux	Urakawa et al. (2020)
NorESM-OC1.2 ^{a,b}	v20211125	1980–2018	No riverine carbon flux	Schwinger et al. (2016)
OCIMv2021 ^a	v20210511	1980–2018	Data assimilation; Abiotic model; Constant circulation; No riverine carbon flux	DeVries (2022)
OCIMv2014	v20210607	1980–2017	CO ₂ flux only; Data assimilation; Abiotic model; Constant circulation; No riverine carbon flux	DeVries (2014)
ORCA1-LIM3-PISCES ^{a,b}	v20211215	1980–2018		Aumont et al. (2015)
ORCA025-GEOMAR ^{a,b}	v20210804	1980–2018	No riverine carbon flux	Kriest and Oschlies (2015)
Planktom12 ^{a,b}	v20220404	1980–2018		Wright et al. (2021)
Arctic_NEMURO-C ^a	DK01M	1979–2018	Arctic only; No riverine carbon flux	Watanabe et al. (2019)
ECCO2-Darwin		2006–2013	Data assimilation; No riverine carbon flux	Manizza et al. (2019)
Atmospheric inversions				
CAMS ^a	v20r2	1979–2020	CO ₂ flux only	Chevallier (2020)
CMS-Flux		2010–2020	CO ₂ flux only	Liu et al. (2021)
CTE	v2021	2001–2020	CO ₂ flux only	van der Laan-Luijkx et al. (2017)
Jena-CarboScope ^a	sEXTocNEET2021	1957–2020	CO ₂ flux only	Rödenbeck et al. (2018)
NISMON-CO ₂	v2021.1	1990–2020	CO ₂ flux only	Niwa et al. (2017)
UoE-in situ		2001–2020	CO ₂ flux only	Feng et al. (2016)

^aDenotes the estimates that are used for the ensemble mean of CO₂ uptake in the Arctic Ocean. ^bDenotes the models that conducted all additional simulations required to decompose the CO₂ fluxes (Sims A to D; see text for details).

linear temporal regression applied to the CO₂ flux in a pre-industrial control simulation with constant pCO_{2a} and climatological-mean atmospheric climate forcing (Sim B). As this drift in the Arctic Ocean surface fluxes is less than 2% of the decadal trend, Sim A without any drift adjustments is used to estimate the long-term mean and seasonal as well as interannual variations in the sea-air CO₂ flux and pCO_{2w} in this study. However, potential constant biases in the CO₂ flux (too large natural uptake or outgassing of CO₂) related to the models not being

Table 2
Ensemble Mean and Ensemble Standard Deviation of the Long-Term Mean Sea-Air CO₂ Flux From 1985 to 2018 in Each Region [TgC yr⁻¹]

Region	Sea-air CO ₂ flux [TgC yr ⁻¹]		
	<i>p</i> CO ₂ products	Ocean models	Atm. inversions
Arctic Ocean	-116.2 ± 4.3 (2)	-91.5 ± 30.0 (14)	-91.1 ± 20.8 (2)
Central Basin	-11.1 ± 5.5 (3)	-9.1 ± 8.4 (14)	-10.8 ± 8.0 (2)
W. Greenland Sea	-13.8 ± 4.3 (3)	-11.4 ± 2.8 (14)	-18.5 ± 9.0 (2)
Baffin Bay	-23.1 ± 4.6 (3)	-14.9 ± 5.3 (14)	-17.4 ± 0.7 (2)
Canadian Arc.	-3.8 (1)	-1.3 ± 1.0 (11)	-1.9 ± 1.9 (2)
Beaufort Shelf	-1.4 ± 0.0 (2)	-1.2 ± 1.2 (11)	-0.6 ± 0.8 (2)
Chukchi Sea	-5.9 ± 2.6 (2)	-5.8 ± 1.7 (13)	-1.0 ± 2.4 (2)
E. Siberian Sea	-2.9 ± 0.0 (2)	-2.1 ± 3.7 (13)	-1.1 ± 1.8 (2)
Laptev Sea	-1.9 ± 0.4 (2)	-1.2 ± 1.8 (13)	-0.6 ± 0.8 (2)
Kara Sea	-10.6 ± 2.4 (2)	-5.0 ± 5.4 (13)	-4.4 ± 3.8 (2)
Barents Sea	-49.4 ± 7.5 (4)	-39.5 ± 11.8 (14)	-34.7 ± 10.8 (2)

Note. Negative values indicate a CO₂ flux into the ocean. The numbers in brackets indicate the number of estimates to calculate the ensemble means. Ensemble means are calculated across the estimates, which cover the full period of 1985–2018 (see Table 1).

fully equilibrated might be larger (Terhaar et al., 2023). Unfortunately, such biases cannot be assessed by these simulations and are hence an intrinsic component of the net CO₂ flux uncertainty in the models. The atmospheric inversions used atmospheric transport models and observed atmospheric CO₂ levels to assess sources and sinks of CO₂. All atmospheric inversions used in this study are the same versions as used in the Global Carbon Budget 2021 (Friedlingstein et al., 2022).

For each estimate, monthly CO₂ fluxes and *p*CO_{2w} were interpolated onto a regular 1° × 1° grid. Regional area-weighted means and spatial integrals were calculated based on the basin mask shown in Figure 1. Long-term and annual means of individual estimates were calculated over the period of 1985–2018, the years for which most estimates provided data. In some cases, products and models did not fully cover this period; these means are then based on data from available years. Ensemble means and ensemble standard deviations of the *p*CO₂ products the ocean biogeochemical hindcast and data assimilation models, and the atmospheric inversions were calculated from 1985 to 2018. The number of estimates used for the ensemble means vary among the regions (see numbers in brackets in Table 2).

The areas where sea-air CO₂ flux and *p*CO_{2w} estimates exist in the individual *p*CO₂ products, ocean biogeochemical hindcast and data assimilation models, or atmospheric inversions are not identical. Several *p*CO₂ products (AOML-EXTRAT, CMEMS-FFNN, NIES-ML3, and Takahashi-clim) have, for example, no estimates in the sea ice covered area (see Figures S2 and S3 in Supporting Information S1). The data coverage along the coastline also differs among the products, models and inversions. To minimize biases due to the differences in area coverage, regional CO₂ flux and *p*CO_{2w} averages were calculated only where data was available for at least 80% of the total region's area (see Table S2 in Supporting Information S1). For example, area averaged values in the Arctic Ocean, the Central Basin, and the Canadian Archipelago are not calculated from AOML-EXTRAT, CMEMS-FFNN, NIES-ML3, and Takahashi-clim as their areal coverage is below 80% in these regions. For the regional CO₂ uptake, first the area-weighted average of flux density was calculated using the areas covered by each estimate, and then it was scaled up using the same area for all data sets. The uncertainty associated with this scaling is determined by comparing scaled regional CO₂ uptakes from minimum coverage and maximum coverage using the estimates which cover the entire area. This is estimated to be smaller than 4%, which is much less than the standard deviation among the estimates.

The specific sea ice concentration (SIC) and sea surface temperature (SST) used as predictor variables in the *p*CO₂ products and those simulated in the ocean biogeochemical hindcast and data assimilation models are used for driver analysis in this study. Part of the *p*CO₂ products and all models included in the RECCAP2 data

compilation provide SIC and SST. For the $p\text{CO}_2$ products that did not provide SIC and SST, Hadley Centre Sea Ice and SST data set (Rayner et al., 2003), National Oceanic and Atmospheric Administration (NOAA)/National Snow and Ice Data Center Climate Data Record of Passive Microwave Sea Ice Concentration version 2 (Meier et al., 2013), and NOAA Optimum Interpolation SST Version 2 (Reynolds et al., 2002) were used for our analysis. SIC and SST data sets in the products are listed in Table S1 of the Supporting Information S1.

2.3. $p\text{CO}_{2w}$ and $p\text{CO}_{2a}$ Observations

Direct $p\text{CO}_{2w}$ observations available in the Surface Ocean CO_2 Atlas (SOCAT) version 6 (Bakker et al., 2016) and the Global Surface $p\text{CO}_2$ Database version 2017 (LDEOV2017; Takahashi et al., 2018) were combined, and binned on a regular $1^\circ \times 1^\circ \times 1$ month grid after removing duplicates and extreme values (see Yasunaka et al., 2018, for the detailed procedure), and used to evaluate the $p\text{CO}_{2w}$ estimates in the $p\text{CO}_2$ product and the ocean biogeochemical hindcast and data assimilation models. The availability of $p\text{CO}_{2w}$ data varies spatially and temporally (Figure S1 in Supporting Information S1). Most of the available data are in the western Greenland Sea, the Beaufort Shelf, the Chukchi Sea, and the Barents Sea, while much less data are available for the Central Basin, the East Siberian Sea, the Laptev Sea, and the Kara Sea. The number of $p\text{CO}_{2w}$ data strongly increased after 2005, but it was still limited in winter.

Zonal mean data for the atmospheric CO_2 mixing ratio ($x\text{CO}_{2a}$) from the NOAA Greenhouse Gas Marine Boundary Layer Reference product (Conway et al., 1994) were interpolated into $1^\circ \times 1^\circ \times 1$ month grid-cells assuming even $x\text{CO}_{2a}$ values across all longitudes, and converted to $p\text{CO}_{2a}$ using SST data from the NOAA Optimum Interpolation SST Version 2 (Reynolds et al., 2002) and sea-level pressure from the US National Centers for Environmental Prediction–Department of Energy Reanalysis 2 (NCEP2) (Kanamitsu et al., 2002).

2.4. Assessment of Components of the Net Sea-Air CO_2 Flux

The sea-air CO_2 flux can be decomposed into multiple components:

$$F_{\text{net}} = F_{\text{ant,ss}} + F_{\text{ant,ns}} + F_{\text{nat,ss}} + F_{\text{nat,ns}}$$

where the subscript ant denotes anthropogenic, nat natural, ss steady state, and ns denotes non-steady state (Hauck et al., 2020).

Most of the ocean biogeochemical hindcast models provide additional simulations that allow quantifying different components of the sea-air CO_2 flux (Table 1). In addition to the historical run with historical time-evolving $p\text{CO}_{2a}$ and historical time-evolving atmospheric climate forcing (Sim A for F_{net}), and the pre-industrial control run with constant $p\text{CO}_{2a}$ and climatological-mean atmospheric climate forcing (Sim B for $F_{\text{nat,ss}}$), two simulations with historical time-evolving $p\text{CO}_{2a}$ and climatological-mean atmospheric climate forcing (Sim C for $F_{\text{ant,ss}} + F_{\text{nat,ns}}$), and constant $p\text{CO}_{2a}$ and historical time-evolving atmospheric climate forcing (Sim D for $F_{\text{nat,ss}} + F_{\text{nat,ns}}$) were performed by most hindcast models.

Here, we decompose the net CO_2 flux (F_{net}) in two ways. The first decomposition split the net CO_2 flux into the flux of natural carbon ($F_{\text{nat,ss}} + F_{\text{nat,ns}}$) and the flux of anthropogenic carbon ($F_{\text{ant,ss}} + F_{\text{ant,ns}}$):

$$\begin{aligned} &\text{Net CO}_2 \text{ flux } (F_{\text{net}} \text{ from Sim A}) \\ &= \text{Natural CO}_2 \text{ flux } (F_{\text{nat,ss}} + F_{\text{nat,ns}} \text{ from Sim D}) \\ &+ \text{Anthropogenic CO}_2 \text{ flux } (F_{\text{ant,ss}} + F_{\text{ant,ns}} \text{ from Sim A} - \text{Sim D}). \end{aligned} \quad (1)$$

In this first decomposition, both the natural and the anthropogenic fluxes do not distinguish between flux components that represent a steady-state and those that are affected by climate change and variability.

The second decomposition splits the net CO_2 flux (F_{net}) into the natural CO_2 flux in steady state ($F_{\text{nat,ss}}$), the CO_2 flux driven by increasing $p\text{CO}_{2a}$ alone (referred to as the CO_2 effect; $F_{\text{ant,ss}}$), and the CO_2 flux due to climate change and variability (referred to as the climate effect; $F_{\text{nat,ns}} + F_{\text{ant,ns}}$):

$$\begin{aligned} &\text{Net CO}_2 \text{ flux } (F_{\text{net}} \text{ from Sim A}) \\ &= \text{Natural CO}_2 \text{ flux in steady state } (F_{\text{nat,ss}} \text{ from Sim B}) \\ &+ \text{CO}_2 \text{ flux by CO}_2 \text{ effect } (F_{\text{ant,ss}} \text{ from Sim C} - \text{Sim B}) \\ &+ \text{CO}_2 \text{ flux by climate effect } (F_{\text{nat,ns}} + F_{\text{ant,ns}} \text{ from Sim A} - \text{Sim C}). \end{aligned} \quad (2)$$

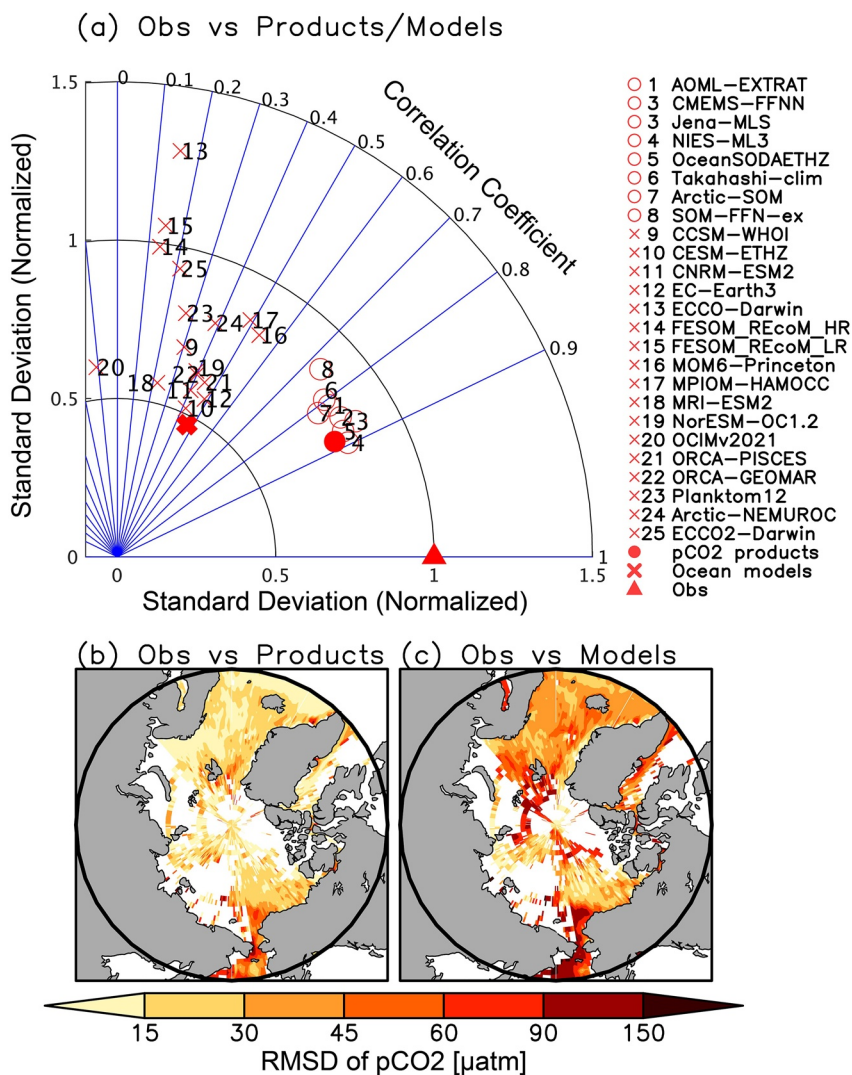


Figure 2. (a) Taylor diagram of $p\text{CO}_{2w}$. The radial distance from the origin represents the standard deviation of $p\text{CO}_{2w}$ in each estimate relative to that of the available observations. The azimuthal angle represents the correlation coefficient of $p\text{CO}_{2w}$ between the individual estimate and the observation. (b, c) Root mean squared difference between observed and ensemble mean $p\text{CO}_{2w}$ from $p\text{CO}_2$ products (b) and ocean biogeochemical models (c). $p\text{CO}_{2w}$ from $p\text{CO}_2$ products and ocean biogeochemical hindcast and data assimilation models were subsampled at the same time and location as the observations.

In this second decomposition, the climate-driven CO_2 flux does not distinguish between fluxes of anthropogenic or natural carbon.

3. Results

3.1. Comparison With Observed Values

The estimates of $p\text{CO}_{2w}$ from the $p\text{CO}_2$ products and the ocean biogeochemical hindcast and data assimilation models were evaluated by comparing them to available observed values of $p\text{CO}_{2w}$ at the same time and location on the $1^\circ \times 1^\circ \times 1$ month grid.

All individual $p\text{CO}_2$ products are better correlated with observed values (correlation coefficients are 0.7–0.9) than most models (correlation coefficients are lower than 0.6; Figure 2a). Both the $p\text{CO}_2$ products and the models underestimate the variability of $p\text{CO}_{2w}$ in time and space. The standard deviations of the $p\text{CO}_2$ products over time and space are about 80% of the standard deviation of the observations. The standard deviations of the ocean

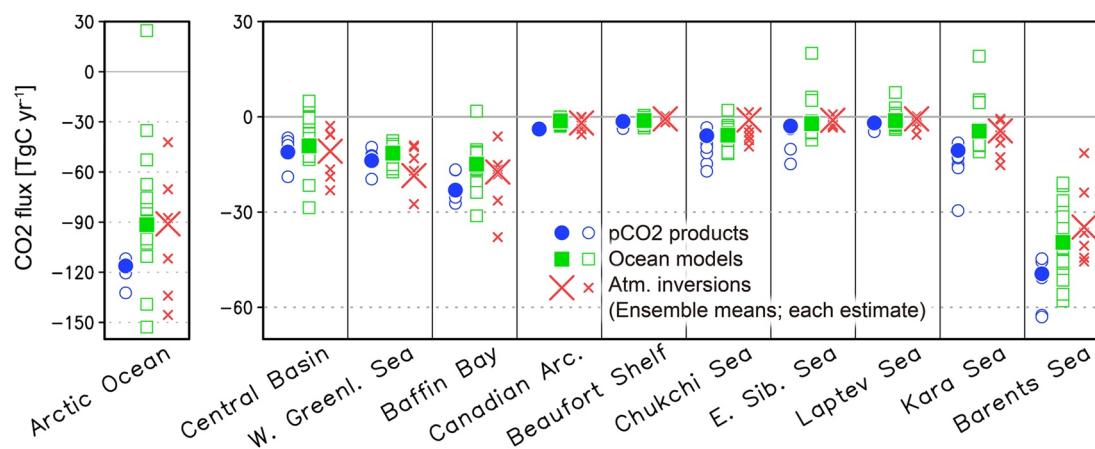


Figure 3. Long-term mean sea-air CO_2 flux. Closed or large marks indicate ensemble means and open or small marks indicate individual estimates (blue circle, $p\text{CO}_2$ products; green square, ocean biogeochemical hindcast and data assimilation models; red cross, atmospheric inversions) averaged over the period of 1985–2018 (or in some cases the longest period covered by the estimate). Negative values indicate a CO_2 flux into the ocean. Ensemble means are calculated across the estimates, which cover the full period of 1985–2018 (see Table 1).

biogeochemical models are mostly smaller than 80% of the observations and often smaller than 60%, while one data assimilation model (ECCO-Darwin) is 130%. The ensemble means of products and models, tend to slightly better correlate with observations than the individual products and models (the correlation coefficient is 0.88 for the ensemble mean of products and 0.47 for that of models), but this comes at the cost of a lower agreement on the magnitude of variability, that is, averaging tends to smooth the values (the standard deviations of the ensemble means are 78% of the observations in the $p\text{CO}_2$ products and 47% in the ocean biogeochemical hindcast and data assimilation models). Differences between the observation and the ensemble means of products and models are particularly large in the Chukchi Sea and around 85°N (root mean squared difference is $30\text{--}90\ \mu\text{atm}$ in the products and $90\text{--}150\ \mu\text{atm}$ in the models in those regions; Figures 2b and 2c).

The better agreement of $p\text{CO}_{2w}$ in the $p\text{CO}_2$ products and observed $p\text{CO}_{2w}$ reflects that the $p\text{CO}_2$ products use the $p\text{CO}_{2w}$ observations as basis for their estimates (and not independent data) and does not ensure a good performance of the $p\text{CO}_2$ products in data-sparse regions (see Figure S1 in Supporting Information S1). Unfortunately, the lack of independent measurements prevents us from quantifying the performance of the $p\text{CO}_2$ products and the ocean biogeochemical hindcast and data assimilation models in data-sparse regions. Furthermore, the monthly means of the observed $p\text{CO}_{2w}$ may not be comparable to the estimated $p\text{CO}_{2w}$ in the products and the models. They are sometimes based on measurements from a single cruise in that month and may not be representative of the monthly mean $p\text{CO}_{2w}$ values in regions with large day-to-day variation and within-grid-cell spatial variability (Yasunaka et al., 2016).

3.2. Long-Term Mean

3.2.1. Sea-Air CO_2 Flux and $p\text{CO}_{2w}$

The long-term mean sea-air CO_2 flux shows that the Arctic Ocean acted as a sink for CO_2 from the atmosphere (Figure 3; Table S2 in Supporting Information S1). Averaged and scaled up, the CO_2 flux over the Arctic Ocean from 1985 to 2018 yields an uptake of $116 \pm 4\ \text{TgC yr}^{-1}$ in the $p\text{CO}_2$ products (average over 2 products), $92 \pm 30\ \text{TgC yr}^{-1}$ in the ocean biogeochemical hindcast and data assimilation models (average over 14 models), and $91 \pm 21\ \text{TgC yr}^{-1}$ in the atmospheric inversions (average over 2 inversions). (Ensemble mean \pm ensemble standard deviation; Figure 3; Tables 1 and 2; Table S1 in Supporting Information S1). All individual estimates except one data assimilation model (OCIMv2014) agree that the Arctic Ocean acted as a sink for atmospheric CO_2 over the 1985 to 2018 period (Figure 3; Table S2 in Supporting Information S1).

The ensemble mean of the regional sea-air CO_2 flux shows ocean uptake larger than the standard deviation in all regions in the $p\text{CO}_2$ products, in most regions in the ocean biogeochemical hindcast and data assimilation models except for the East Siberian Sea, the Laptev Sea, and the Kara Sea, and in most regions in the atmospheric inversions except for the Chukchi Sea, the East Siberian Sea, and the Laptev Sea (Figure 3; Table 2).

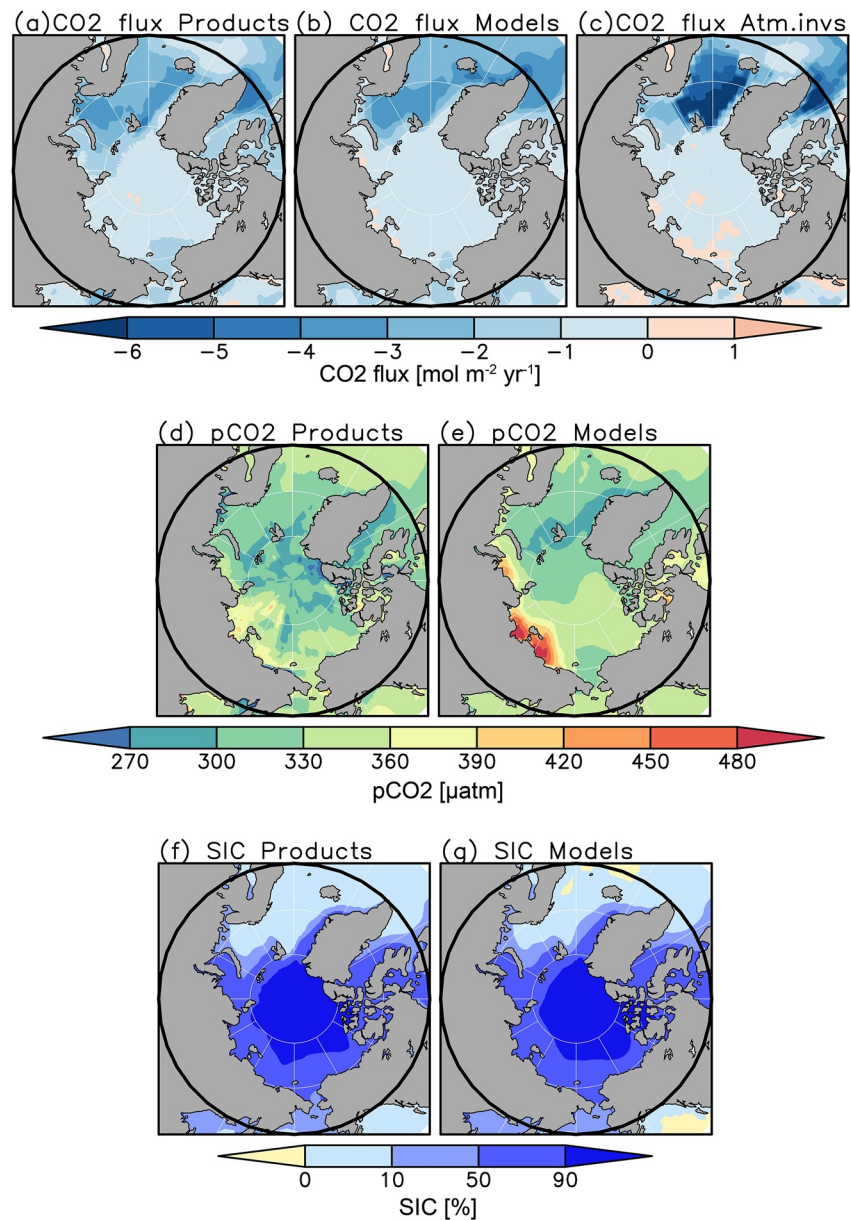


Figure 4. Long-term mean CO_2 flux (a–c), $p\text{CO}_{2w}$ (d, e), and SIC (f, g) in the period of 1985–2018 for ensemble means of $p\text{CO}_2$ products (a, d, f), ocean biogeochemical hindcast and data assimilation models (b, e, g), and atmospheric inversions (c). Negative values indicate CO_2 flux into the ocean in panels (a–c). Ensemble means are calculated across the estimates, which cover the full period of 1985–2018 (see Table 1).

Both the $p\text{CO}_2$ products and the models show the largest uptake per unit area in the Barents Sea (sea-air CO_2 flux $< -3 \text{ mol m}^{-2} \text{ yr}^{-1}$), and smaller to medium uptake in the western Greenland Sea, the Baffin Bay, and the Chukchi Sea (sea-air CO_2 flux -2 to $-1 \text{ mol m}^{-2} \text{ yr}^{-1}$; Figures 4a and 4b). Some individual models even show outgassing of CO_2 in the Central Basin (FESOM_REcoM_HR and FESOM_REcoM_LR), the Baffin Bay (OCIMv2014), and the coastal areas such as the Beaufort Shelf (CAMS), the Chukchi Sea (ECCO-Darwin and CAMS), the East Siberian Sea (FESOM_REcoM_HR, FESOM_REcoM_LR, OCIMv2014 and CAMS), the Laptev Sea (FESOM_REcoM_HR, FESOM_REcoM_LR, OCIMv2014, Planktom12 and CAMS), and the Kara Sea (FESOM_REcoM_HR, FESOM_REcoM_LR, OCIMv2014 and Planktom12) (Figures S2 and S3; Table S2 in Supporting Information S1).

The spatial distribution of the standard deviation of CO_2 flux among the individual estimates are different among the categories of estimates; it is large ($>1 \text{ mol m}^{-2} \text{ yr}^{-1}$) in the Barents, the Chukchi Sea, and around 80°N in

the $p\text{CO}_2$ products, in the Barents Sea and the coastal region of the Kara Sea and the Laptev Sea in the ocean biogeochemical hindcast and data assimilation models, and in the western Greenland Sea and the Barents Sea in the atmospheric inversions (Figures S4a–S4c in Supporting Information S1).

In line with the overall negative sea-air CO_2 flux in the Arctic Ocean, the annual mean of $p\text{CO}_{2w}$ from 1985 to 2018 is lower than the annual mean of the $p\text{CO}_{2a}$ ($\sim 390 \mu\text{atm}$) in almost all regions except for the coastal region along the Eurasian Continent (Figures 4d and 4e). The standard deviation among the individual estimates is smaller in the $p\text{CO}_2$ products than in the ocean biogeochemical hindcast and data assimilation models (Figures S4d and S4e in Supporting Information S1). For the $p\text{CO}_2$ products, the standard deviation is smaller than $30 \mu\text{atm}$ except for smaller areas in the coastal and sea ice edge regions. On the other hand, the standard deviation in the models is more than $90 \mu\text{atm}$ in the coastal region along the Eurasian coast due to the high $p\text{CO}_{2w}$ ($>480 \mu\text{atm}$) in several models there. The region where the standard deviation is large corresponds to where the number of observations is limited (Figure S1 in Supporting Information S1).

The spatial patterns of the sea-air CO_2 flux are different from those of the $p\text{CO}_{2w}$ and correspond to the SIC (Figure 4). The largest uptake across all products occurs in the Barents Sea, of which $>50\%$ remains ice free even in winter (Árthun, et al., 2012). Moreover, this is a region where $p\text{CO}_{2w}$ is substantially reduced because of the large heat loss from the Atlantic waters that flow from the southwest (Lundberg & Haugan, 1996). Medium CO_2 uptake in the western Greenland Sea, the Baffin Bay and the Chukchi Sea corresponds to moderate SIC and low $p\text{CO}_{2w}$. Although very low $p\text{CO}_{2w}$ ($<330 \mu\text{atm}$) is estimated for the Central Basin, the CO_2 uptake is small as thick sea ice does not allow for sea-air gas exchange. In the East Siberian Sea, the Laptev Sea and the Kara Sea, the CO_2 uptake is small or even outgassing in some biogeochemical hindcast and data assimilation models because $p\text{CO}_{2w}$ is relatively high due to large influxes of organic and inorganic carbon from rivers and coastal erosion (Figures 4a–4e; Figures S2 and S3 in Supporting Information S1; Anderson et al., 2009; Manizza et al., 2011; Tank et al., 2012; Tanski et al., 2021; Vonk et al., 2012).

3.2.2. Natural and Anthropogenic Sea-Air CO_2 Flux and the Climate and CO_2 Effect

The net Arctic Ocean CO_2 uptake of $93 \pm 27 \text{ TgC yr}^{-1}$ in the hindcast models (F_{net} ; number is different from that in Table 2 because the uptake here is the average only over those models that have also provided Sims B, C and D; see Table 1) is the sum of large uptake of natural carbon ($F_{\text{nat,ss}} + F_{\text{nat,ns}}$; $74 \pm 23 \text{ TgC yr}^{-1}$; $80\% \pm 25\%$ of the net uptake) and smaller uptake of anthropogenic carbon ($F_{\text{ant,ss}} + F_{\text{ant,ns}}$; $19 \pm 6 \text{ TgC yr}^{-1}$; $20\% \pm 22\%$) (Figure 5). Regionally, the relative importance of the flux of anthropogenic carbon is large on the North American side from the Baffin Bay ($36\% \pm 12\%$) to the Beaufort Shelf ($34\% \pm 12\%$) and small on the Eurasian continent side from the Chukchi Sea ($18\% \pm 16\%$) to the Barents Sea ($14\% \pm 5\%$).

The net sea-air CO_2 flux (F_{net}) can also be divided into the steady state natural flux ($F_{\text{nat,ss}}$), the CO_2 fluxes due to the atmospheric CO_2 increase alone ($F_{\text{ant,ss}}$), and the CO_2 fluxes caused by climate change and variability ($F_{\text{nat,ns}} + F_{\text{ant,ns}}$; Figure 5). The background steady state natural flux accounts for the largest part of the net Arctic Ocean CO_2 uptake ($65 \pm 14 \text{ TgC yr}^{-1}$; $70\% \pm 15\%$ of the net uptake), and is enhanced by $18 \pm 5 \text{ TgC yr}^{-1}$ ($19\% \pm 5\%$) via the CO_2 effect and by $10 \pm 17 \text{ TgC yr}^{-1}$ ($11\% \pm 18\%$) via the climate effect. The anthropogenic CO_2 uptake in the Arctic Ocean (19 TgC yr^{-1}) is almost fully due to the CO_2 effect (18 TgC yr^{-1}). The climate effect is split into the climate effect on the anthropogenic flux ($19 - 18 = 1 \text{ TgC yr}^{-1}$) and the climate effect on the natural flux in the non-steady state ($10 - 1 = 9 \text{ TgC yr}^{-1}$). Regionally, the climate effect is on average almost nonexistent in the western Greenland Sea, the Baffin Bay, and the Beaufort Shelf although it varies strongly among the individual models. In the remaining regions, the climate effect is of similar magnitude or even larger than the CO_2 effect. In contrast to the Arctic Ocean, the CO_2 effect is much larger than the climate effect in the Southern Ocean (the other polar ocean; Hauck et al., 2023) and the global ocean where the CO_2 flux via the CO_2 effect is 2.1 PgC yr^{-1} of uptake and the flux from the climate effect is 0.2 PgC yr^{-1} of outgassing, respectively (DeVries et al., 2023). The Arctic Ocean is thus a unique ocean basin where climate change plays a role of similar magnitude as the increase in atmospheric CO_2 in controlling the sea-air fluxes of CO_2 .

The similar strength of the CO_2 effect and the climate effect in the Arctic Ocean requires a relatively strong climate effect and a relatively weak CO_2 effect compared to other ocean basins. The climate effect is strong in the Arctic due to fast warming (Arctic Amplification; Meredith et al., 2019; Screen & Simmonds, 2010) and the rapid reduction in sea ice coverage that increases the amount of open water and the potential of sea-air CO_2 exchange. Furthermore, the relatively weak CO_2 effect may be caused by the inflowing surface waters from the

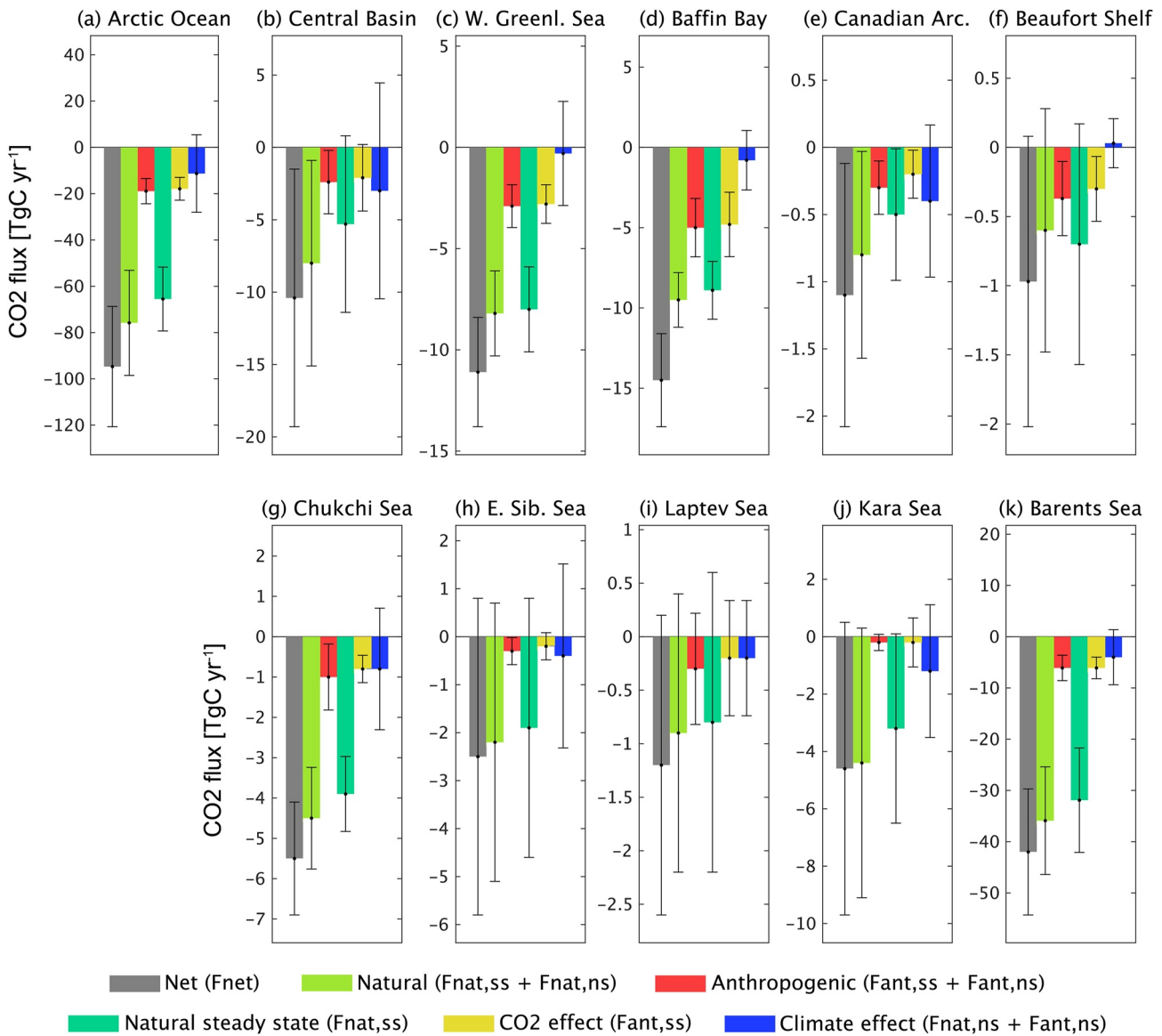


Figure 5. Decomposition of the long-term mean CO₂ flux (F_{net} ; gray) into the natural CO₂ flux ($F_{\text{nat,ss}} + F_{\text{nat,ns}}$; light green) and the anthropogenic CO₂ flux ($F_{\text{ant,ss}} + F_{\text{ant,ns}}$; red), and into the natural CO₂ flux in steady state ($F_{\text{nat,ss}}$; aqua), and the CO₂ flux attributed to the CO₂ effect ($F_{\text{ant,ss}}$; yellow) and the climate effect ($F_{\text{nat,ns}} + F_{\text{ant,ns}}$; blue). Negative values indicate CO₂ flux into the ocean. Error bars denote the standard deviation of the flux components across the ensemble of individual ocean biogeochemical hindcast models.

Atlantic and Pacific Ocean that have already taken up the anthropogenic CO₂ in the Pacific and Atlantic Ocean and thus decrease the importance of the anthropogenic CO₂ flux and hence the CO₂ effect in the Arctic Ocean (Olsen et al., 2015; Terhaar, Orr, Gehlen, et al., 2019).

3.3. Seasonal Cycle

The CO₂ uptake in the Arctic Ocean is largest in late summer and early autumn (August–October), and smallest in winter and spring (January–May) (Figure 6a). The phasing of the seasonal cycle is similar in all subregions of the Arctic Ocean (Figures 6b–6j) except the Barents Sea, which has a relatively constant CO₂ uptake throughout the year (Figure 6k). The seasonal amplitude of the sea-air CO₂ flux is large in the western Greenland Sea, the Baffin Bay, the Chukchi Sea, and the Kara Sea (mostly >2 mol m⁻² yr⁻¹; Figures 6c, 6d, 6g, and 6j, respectively), and small in the Central Basin and the Canadian Archipelago (mostly <1 mol m⁻² yr⁻¹; Figures 6b and 6e). OCIMv2014 has no seasonal cycle of CO₂ flux because of the annual time steps of this model (DeVries, 2014).

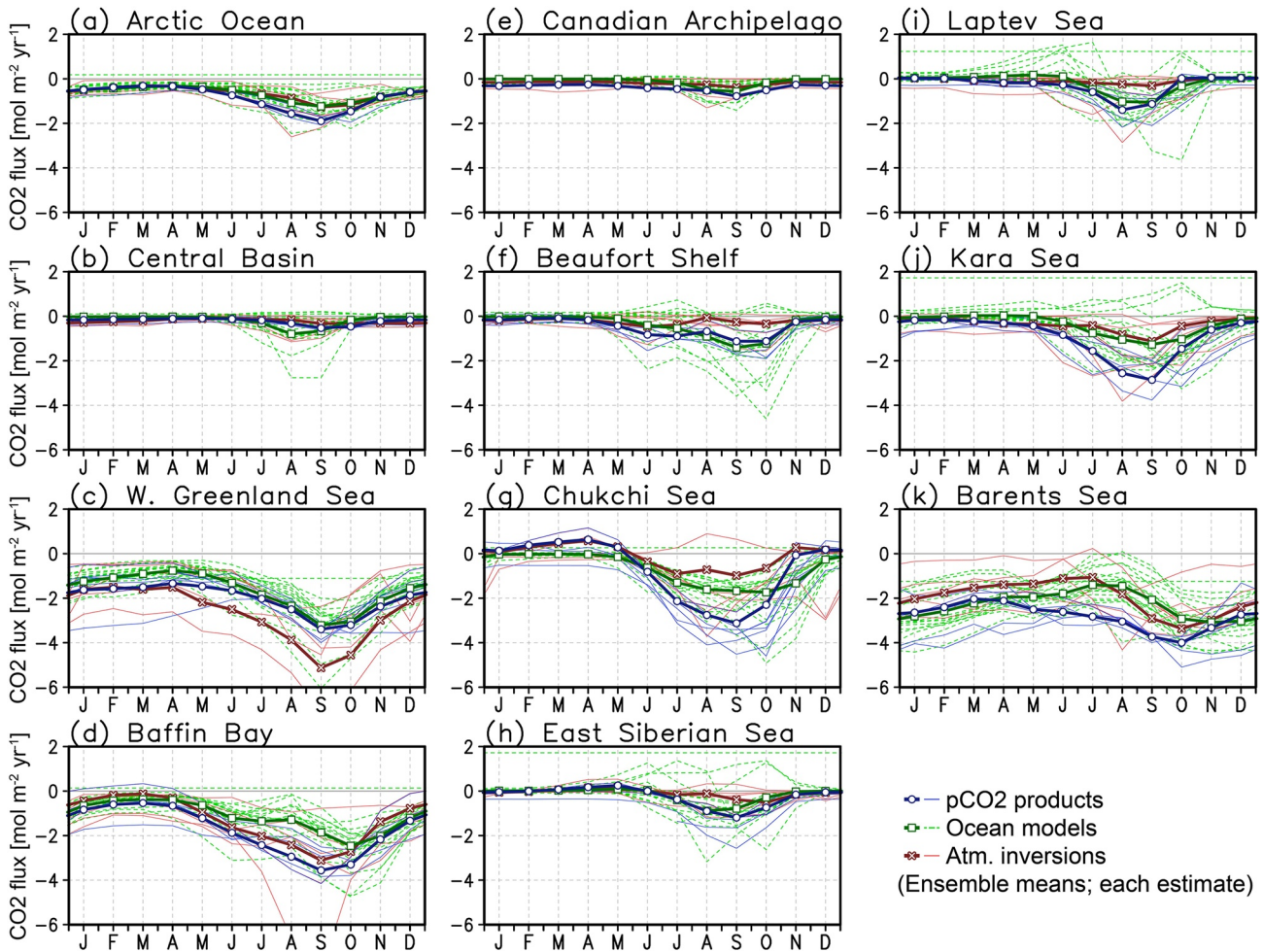


Figure 6. Monthly climatology of CO₂ flux averaged over the period of 1985–2018 (or the longest period available). Thick lines with marks indicate ensemble means, and thin lines indicate individual estimates (blue and circle, *p*CO₂ products; green and square, ocean biogeochemical hindcast and data assimilation models; red and cross, atmospheric inversions). Negative values indicate CO₂ flux into the ocean. Ensemble means are calculated across the estimates, which cover the full period of 1985–2018 (see Table 1).

The seasonal amplitude of the CO₂ flux tends to be larger in the *p*CO₂ products than in the ocean biogeochemical hindcast and data assimilation models (Figure 6). The largest differences in CO₂ uptake between *p*CO₂ products and the models occur in summer in the Baffin Bay, the Chukchi Sea, the Kara Sea, and the Barents Sea (Figures 6d, 6g, 6j, and 6k, respectively). Seasonal variation is small in the atmospheric inversions in the Beaufort Shelf, the Chukchi Sea, the Laptev Sea and the Kara Sea (Figures 6f, 6g, 6i, and 6j, respectively). The phasing of the seasonal cycle in the Barents Sea differs among the categories of estimates; CO₂ uptake based on the *p*CO₂ products is on average largest in October and smallest in April, while the models and the atmospheric inversions have their summer minimum uptake in July (Figure 6k). Large differences in the phasing of the seasonal cycle also exist in several ocean biogeochemical hindcast models (FESOM_REcoM_HR, FESOM_REcoM_LR, Planktom12, and Arctic_NEMRO-C) that show CO₂ release in the East Siberian Sea, the Laptev Sea, and/or the Kara Sea from spring to autumn (Figures 6h–6j). CAMS shows CO₂ release in summer in the Chukchi Sea and the East Siberian Sea (Figures 6g and 6h, respectively).

The average *p*CO_{2w} in the Arctic Ocean peaks in late winter to early spring (February–May), and reaches a minimum in summer (July–August) (Figure 7a), which slightly precedes the seasonal cycle of the sea-air CO₂ flux (Figure 6a). For the *p*CO₂ products, this pattern is apparent in all subregions, but the ocean biogeochemical hindcast and data assimilation models simulate highest *p*CO_{2w} levels in the Barents Sea and the Baffin Bay during mid-summer (Figures 7d and 7k). *p*CO_{2w} in the Chukchi Sea in spring is higher in the *p*CO₂ products than in the models (Figure 7g). A few ocean biogeochemical hindcast model estimates show high *p*CO_{2w} (>500 μatm)

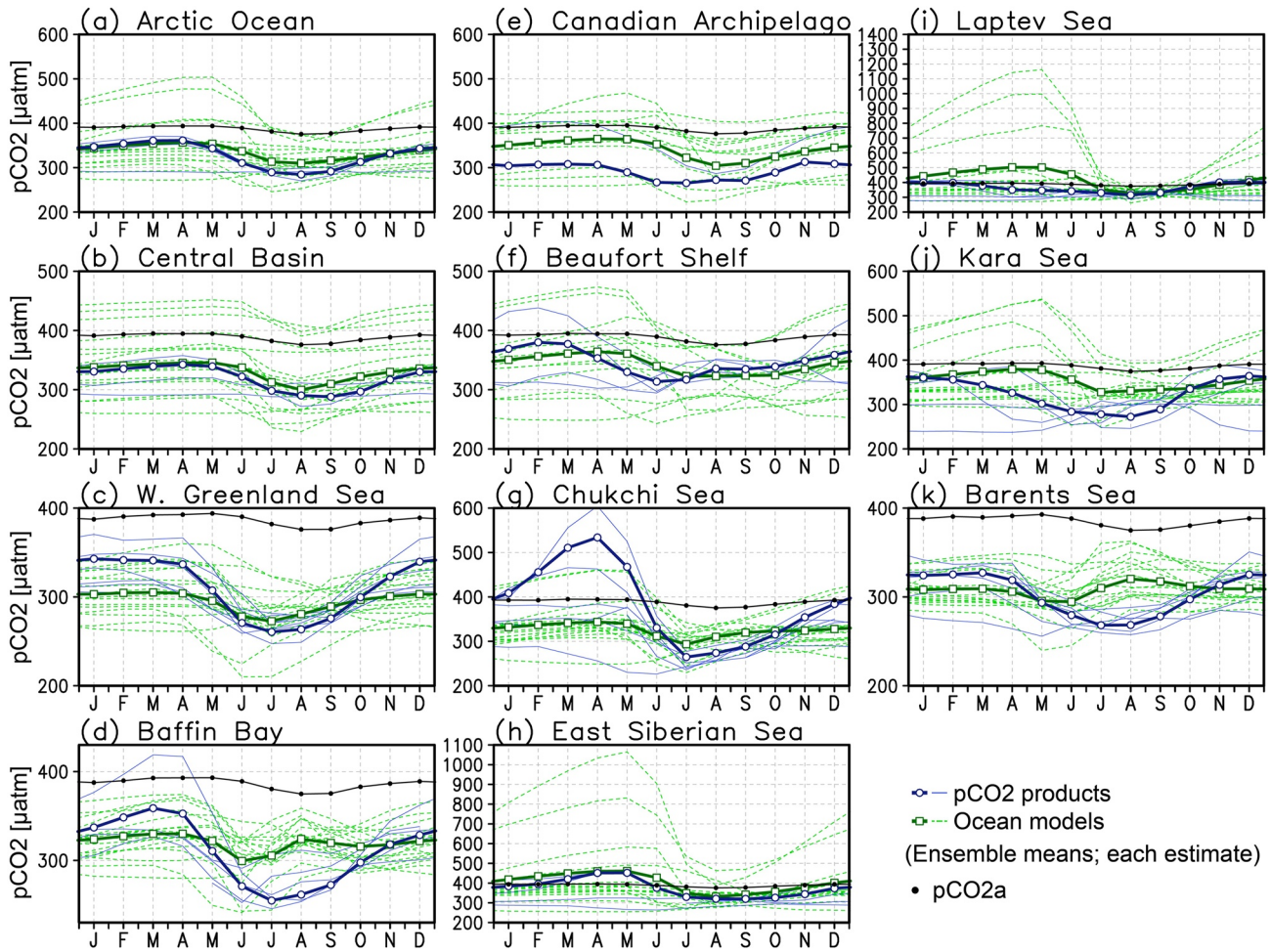


Figure 7. Monthly climatology of $p\text{CO}_{2w}$ averaged over the period of 1985–2018 (or the longest period available). Tick lines with marks indicate ensemble means, and thin lines indicate individual estimates (blue and circle, $p\text{CO}_2$ products; green and square, ocean biogeochemical hindcast and data assimilation models), and observed $p\text{CO}_{2a}$ (black dot). Ensemble means are calculated across the estimates, which cover the full period of 1985–2018 (see Table 1).

values in winter and spring in the East Siberian Sea, the Laptev Sea, and the Kara Sea (FESOM_REcoM_HR, FESOM_REcoM_LR, and Arctic_NEMROC; Figures 7h–7j).

The seasonal cycle of the sea-air CO_2 flux correlates with SIC in all regions both in the $p\text{CO}_2$ products and the ocean biogeochemical hindcast and data assimilation models but the Barents Sea; CO_2 uptake is large when SIC is low in summer, and it is small when sea ice covers the ocean (Figures 6 and 8). Relative seasonal amplitudes of the CO_2 flux correspond well with those of the SIC; the seasonal amplitude of the CO_2 flux is large where that of the SIC is large (Figure S5 in Supporting Information S1). In essence, the seasonal amplitudes of SIC alone explain the CO_2 flux variability, which is expected since the CO_2 flux is generally calculated assuming that it is proportionally inhibited by SIC. In the Barents Sea, the seasonal cycle of CO_2 flux in the $p\text{CO}_2$ products is in phase with SIC but in the models it is modulated by high $p\text{CO}_{2w}$ in summer.

The discrepancy between the $p\text{CO}_2$ products and the ocean biogeochemical hindcast and data assimilation models is discussed in Section 4.2.2.

3.4. Decadal Trends

3.4.1. Sea-Air CO_2 Flux and $p\text{CO}_{2w}$

The annual CO_2 uptake increases from 1985 to 2018 in almost all regions (Figures 9, 10a, and 10b; Table S3 in Supporting Information S1). The increase in the CO_2 uptake per unit area is particularly large in the Barents Sea, the

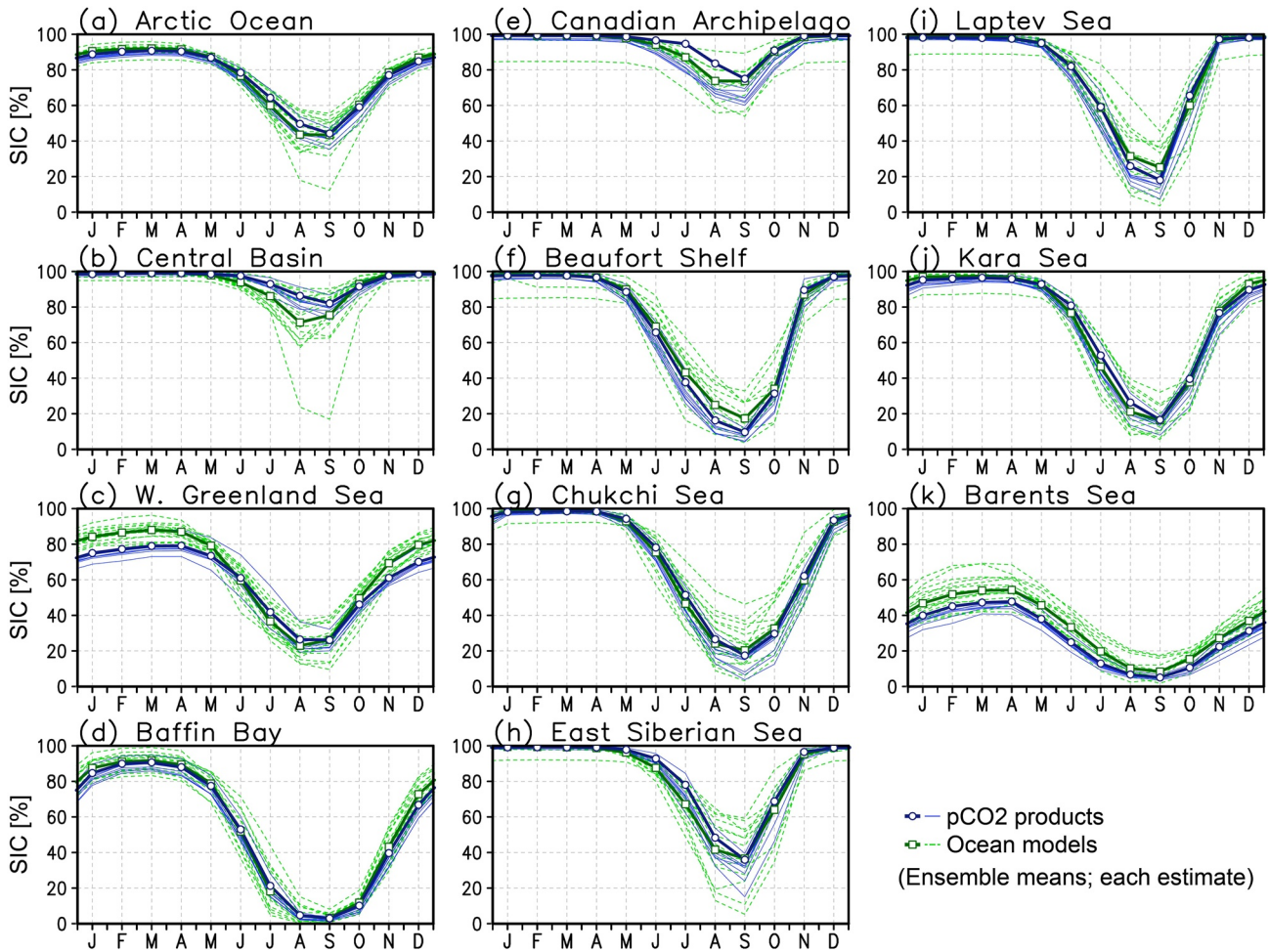


Figure 8. Monthly climatology of SIC averaged over the period of 1985–2018 (or the longest period available). Thick lines with marks indicate ensemble means, and thin lines indicate individual estimates (blue and circle, $p\text{CO}_2$ products; green and square, ocean biogeochemical hindcast and data assimilation models). Ensemble means are calculated across the estimates, which cover the full period of 1985–2018 (see Table 1).

Kara Sea, and the western Greenland Sea (linear slopes of sea-air CO_2 flux $< -0.2 \text{ mol}^{-1} \text{ m}^{-2} \text{ yr}^{-1} \text{ dec}^{-1}$; Figures 9c, 9j, 9k, 10a, and 10b). During the 1985–2018 period, the trend in the CO_2 uptake integrated over the entire Arctic Ocean is $31 \pm 13 \text{ TgC yr}^{-1} \text{ dec}^{-1}$ in the $p\text{CO}_2$ products, $10 \pm 4 \text{ TgC yr}^{-1} \text{ dec}^{-1}$ in the ocean biogeochemical hindcast and data assimilation models, and $32 \pm 16 \text{ TgC yr}^{-1} \text{ dec}^{-1}$ in the atmospheric inversions (Table S3 in Supporting Information S1). In the $p\text{CO}_2$ products and the inversions, the uptake trend in the Arctic Ocean (especially in the Kara Sea, the Laptev Sea, the East Siberian Sea and the Barents Sea in the $p\text{CO}_2$ products, and in the Kara Sea and the Barents Sea in the inversions) accelerated in the recent period, while such acceleration is not simulated by the models (Table S3 in Supporting Information S1). In the models, a positive trend in CO_2 flux (decrease in CO_2 uptake or increase in CO_2 release) is observed in the coastal region off the Eurasian Continent (Figure 10b).

The $p\text{CO}_{2w}$ increases with the atmospheric $p\text{CO}_2$ in all regions (Figure 11). During the 1985–2018 period, the trend in $p\text{CO}_{2w}$ integrated over the entire Arctic Ocean is $7 \pm 10 \mu\text{atm dec}^{-1}$ in the $p\text{CO}_2$ products, and $18 \pm 3 \mu\text{atm dec}^{-1}$ in the ocean biogeochemical hindcast and data assimilation models. The trend in $p\text{CO}_{2w}$ in both the $p\text{CO}_2$ products and the models is smaller than the atmospheric $p\text{CO}_2$ increase ($\sim 21 \mu\text{atm dec}^{-1}$; Figures 10c–10e and 11). In the $p\text{CO}_2$ products, the $p\text{CO}_{2w}$ trend is especially small in the Central Basin, the Chukchi Sea, the East Siberian Sea and the Kara Sea ($< 10 \mu\text{atm dec}^{-1}$). In the models, it is larger than $15 \mu\text{atm dec}^{-1}$ in almost all regions except for coastal parts of the Kara Sea and the East Siberian Sea. The discrepancy between the trends in the $p\text{CO}_2$ products and the ocean biogeochemical hindcast and data assimilation models is discussed in Section 4.2.3.

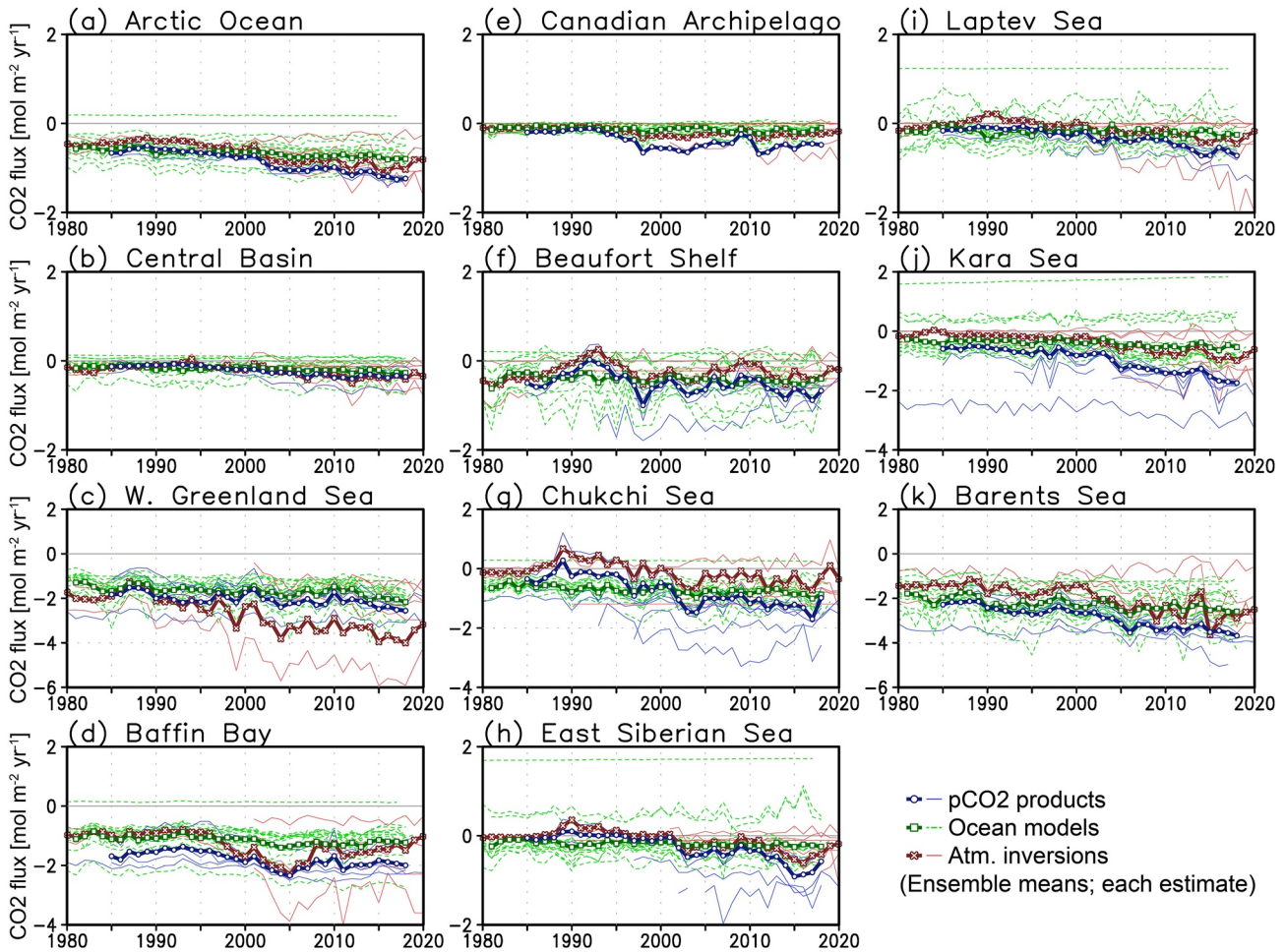


Figure 9. Annual mean CO₂ flux. Thick lines with marks indicate ensemble means, and thin lines indicate individual estimates (blue and circle, *p*CO₂ products; green and square, ocean biogeochemical hindcast and data assimilation models; red and cross, atmospheric inversions). Negative values indicate the CO₂ flux into the ocean. Ensemble means are calculated across the estimates, which cover the full period of 1985–2018 (see Table 1).

3.4.2. Drivers of the Decadal Trends

The spatial patterns of the trend in sea-air CO₂ flux are similar to the SIC trend in both the *p*CO₂ products and the ocean biogeochemical hindcast and data assimilation models (Figures 9, 10, and 12). The largest increase in the CO₂ uptake occurs in regions with extensive sea ice loss, in particular the Barents Sea and the Kara Sea. In these two regions of the Arctic Ocean, the largest reduction in SIC (>5% dec⁻¹) is observed. The trend in CO₂ flux relative to the long-term mean corresponds well with that in the SIC (Figure S6 in Supporting Information S1) except for the coastal region off the Eurasian Continent, indicating that a decrease in the SIC can explain most of the CO₂ flux increase in the Arctic Ocean. Furthermore, smaller trend in CO₂ uptake in models than in *p*CO₂ products also corresponds with difference in the SIC trend. In the coastal region off the Eurasian Continent, in the *p*CO₂ products, the increase in the CO₂ uptake is larger than the decrease in SIC (Figures S6a and S6d in Supporting Information S1) since a small *p*CO_{2w} increase also intensifies the CO₂ uptake (Figure 10d). In the models, the *p*CO_{2w} increase causes a change in the direction of CO₂ flux in some coastal areas off the Eurasian Continent by ocean uptake to release (Figures 4b and 10e; Figure S6b in Supporting Information S1).

A correspondence between the trends in sea-air CO₂ flux and SIC can be seen in each month in both the *p*CO₂ products and the ocean biogeochemical hindcast and data assimilation models (Figure 13). The CO₂ uptake averaged over the Arctic Ocean increases all year round, while on the regional scale the increase occurs in different seasons because the decrease in SIC varies regionally and seasonally (Árthun et al., 2020; Onarheim et al., 2018). In the *p*CO₂ products, for most of the subregions except for the Barents Sea, the largest loss of SIC is observed in summer and autumn, such that the increase in CO₂ uptake is strongest in that season. In the Barents Sea, the CO₂ uptake

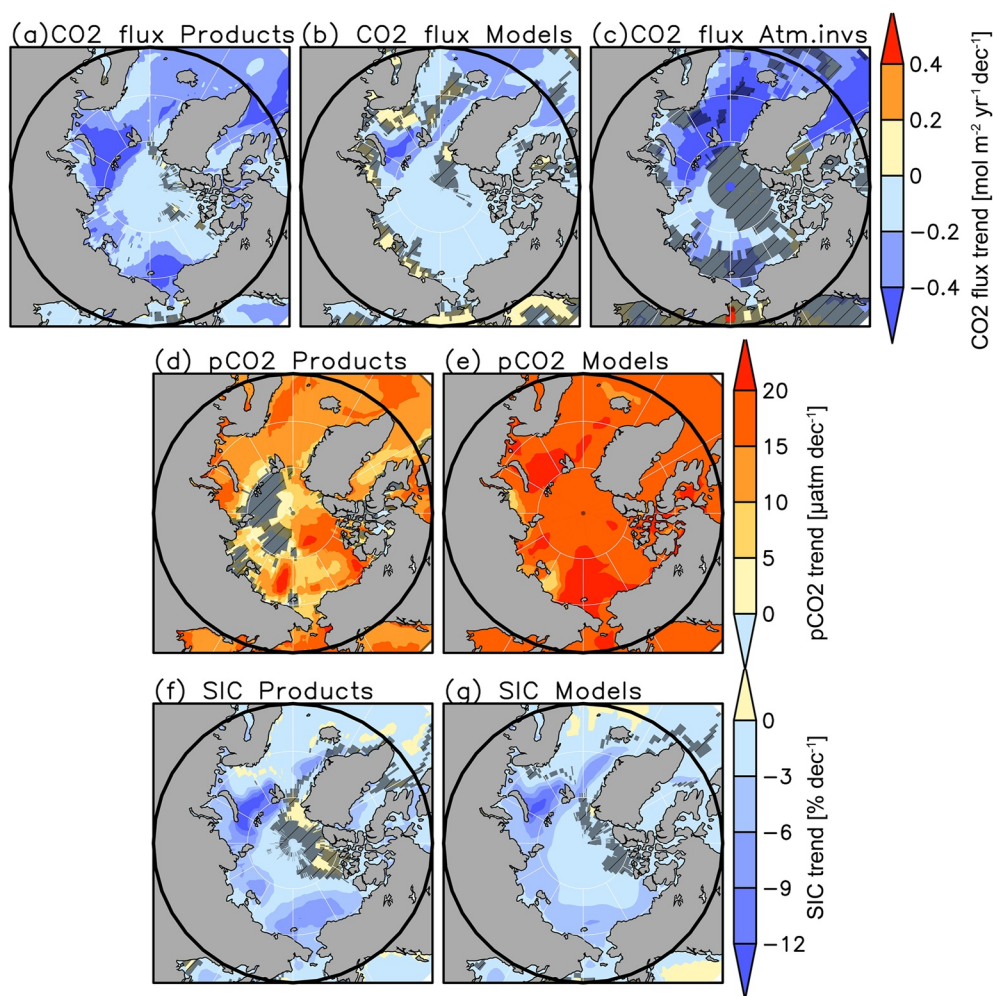


Figure 10. Trend over 1985–2018 for ensemble mean CO_2 flux, $p\text{CO}_{2w}$, and SIC from the $p\text{CO}_2$ products, the ocean biogeochemical hindcast and data assimilation models, and the atmospheric inversions. Negative values indicate increasing CO_2 flux into the ocean in panels (a) and (b). Darker hatched areas represent values in grids where less than two third of the estimates show the same sign of the trend. Ensemble means are calculated across the estimates, which cover the full period of 1985–2018 (see Table 1).

increase shows no particular seasonal pattern; in winter it is driven by the loss of sea ice and in summer it is driven by relatively small $p\text{CO}_{2w}$ growth rates. The SIC trends in the ocean biogeochemical and data assimilation models are similar but smaller in summer than the observed ones. The trend in $p\text{CO}_{2w}$ is larger in the models in almost all months and all regions. As a result, the trends in the CO_2 uptake in the models are much smaller than in the $p\text{CO}_2$ products, as was the case for the annual mean described in Section 3.4.1. This is further discussed in Section 4.2.3.

A dominance of the climate change effect, which includes the impact of the SIC decrease, on the CO_2 flux trend can be inferred from comparing the flux in the four simulations of the ocean biogeochemical hindcast models (Figure 14). In terms of the model ensemble mean, the CO_2 effect ($F_{\text{ant,ss}}$) intensifies the CO_2 uptake (i.e., the CO_2 flux via the CO_2 effect is negative) in all regions and for each year throughout the 1985–2018 period (yellow ribbons in Figure 14), while the climate effect ($F_{\text{nat,ns}} + F_{\text{ant,ns}}$) suppresses the CO_2 uptake (i.e., the CO_2 flux via the climate effect is positive) in some years at every region (hatches in Figure 14). Both effects show a negative trend of CO_2 flux with time, thus contributing to the increase in the net CO_2 uptake. Integrated over the entire Arctic Ocean, $77\% \pm 38\%$ of the trend in the net CO_2 uptake over time is caused by climate change effect on natural and anthropogenic CO_2 , while $25\% \pm 9\%$ is driven by increasing atmospheric CO_2 in the steady state (excess 2% is the trend in the natural CO_2 flux in the steady state ($F_{\text{nat,ss}}$), which would be the model drift). The climate change effect on the CO_2 flux trends tends to be more important in regions of the high Arctic Ocean (the Barents Sea, the Kara Sea, the Laptev Sea, the East-Siberian Sea, the Chukchi Sea, the Canadian Archipelago, and the

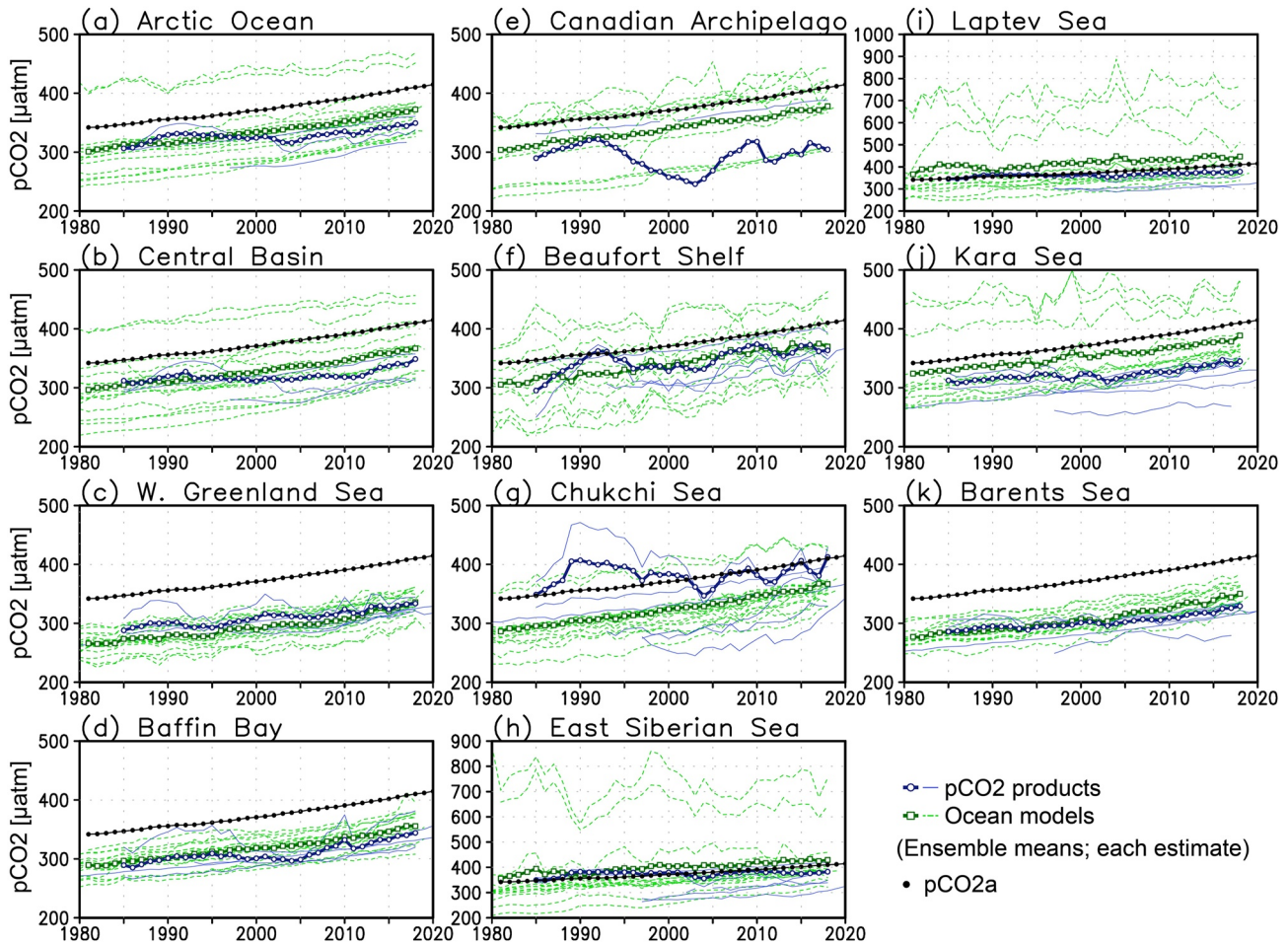


Figure 11. Annual mean $p\text{CO}_{2w}$. Thick lines with marks indicate ensemble means, and thin lines indicate individual estimates (blue and circle, $p\text{CO}_2$ products; green and square, ocean biogeochemical hindcast and data assimilation models) and observed $p\text{CO}_{2a}$ (black dot). Ensemble means are calculated across the estimates, which cover the full period of 1985–2018 (see Table 1).

Central Basin; >70%), whereas the increase in atmospheric CO_2 is more important in southern regions like the Baffin Bay ($84\% \pm 40\%$) and the western Greenland Sea ($52\% \pm 20\%$). The strong climate-induced CO_2 fluxes in the Arctic Ocean (Section 3.2) have become even more important in recent years.

Another decomposition of the Arctic Ocean CO_2 uptake shows $65\% \pm 29\%$ of the increase in the Arctic Ocean CO_2 uptake over time is caused by the natural flux components ($F_{\text{nat,ss}} + F_{\text{nat,ns}}$), while $35\% \pm 18\%$ is driven by anthropogenic components ($F_{\text{ant,ss}} + F_{\text{ant,ns}}$; Figure S7 in Supporting Information S1). Since the anthropogenic component (35%) includes both the CO_2 effect and the climate effect on the anthropogenic CO_2 ($F_{\text{ant,ss}}$ and $F_{\text{ant,ns}}$, respectively), it is bigger than the 25% of the CO_2 effect alone.

4. Discussion

4.1. Comparison With the Previous Estimates

Previous estimates of Bates and Mathis (2009), Schuster et al. (2013), and Yasunaka et al. (2018) were determined for the Arctic Ocean without the western Greenland Sea and the Baffin Bay. When excluding these regions, the here synthesized estimate of the Arctic Ocean CO_2 uptake from 1985 to 2018 reduces to $84 \pm 1 \text{ TgC yr}^{-1}$ in the $p\text{CO}_2$ products, $65 \pm 25 \text{ TgC yr}^{-1}$ in the ocean biogeochemical models, and $55 \pm 30 \text{ TgC yr}^{-1}$ in the atmospheric inversion (Table 2). The estimates from all categories are both larger than their respective estimates in the first implementation of RECCAP ($30 \pm 30 \text{ TgC yr}^{-1}$, $50 \pm 30 \text{ TgC yr}^{-1}$, and $40 \pm 20 \text{ TgC yr}^{-1}$, respectively; Schuster et al., 2013). However, the estimates here are smaller than other estimates ($81\text{--}199 \text{ TgC yr}^{-1}$, Bates &

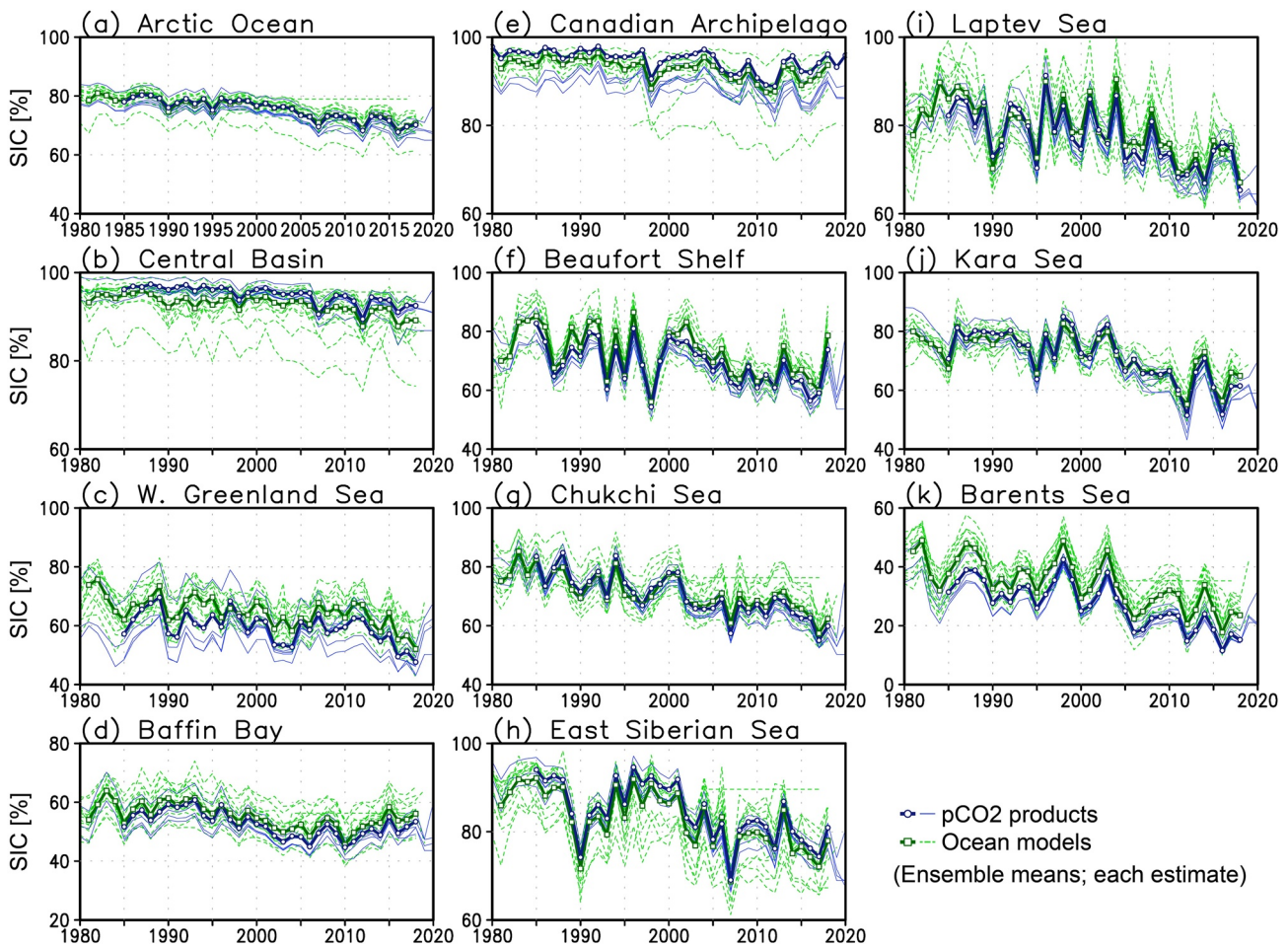


Figure 12. Annual mean SIC. Thick lines with marks indicate ensemble means, and thin lines indicate individual estimates (blue and circle, $p\text{CO}_2$ products; green and square, ocean biogeochemical hindcast and data assimilation models). Ensemble means are calculated across the estimates, which cover the full period of 1985–2018 (see Table 1).

Mathis, 2009, $180 \pm 130 \text{ TgC yr}^{-1}$, Yasunaka et al., 2018) but agree within their uncertainties. Although average periods are different among the studies (before 2004 in Bates and Mathis (2009); 1990–2009 in Schuster et al. (2013); 1997–2014 in Yasunaka et al. (2018)), the different time periods cannot explain the discrepancies between the estimates because the year-to-year variation and the trend in the CO_2 uptake are smaller than the identified discrepancies (Figure 9; Table S3 in Supporting Information S1). In this study and the first phase of RECCAP, the standard deviations and the median absolute deviation across the estimates are used to show the range of estimates, but uncertainties may be larger due to common biases or weaknesses across the entire estimates.

The CO_2 uptake in the Barents Sea in the present study is estimated to be $2.8 \pm 0.9 \text{ mol m}^{-2} \text{ yr}^{-1}$ in the $p\text{CO}_2$ products, $2.3 \pm 0.7 \text{ mol m}^{-2} \text{ yr}^{-1}$ in the ocean biogeochemical hindcast and data assimilation models, and $2.0 \pm 0.7 \text{ mol m}^{-2} \text{ yr}^{-1}$ in the atmospheric inversions, which are in the center of previous studies from 4.4 to $0.7 \text{ mol m}^{-2} \text{ yr}^{-1}$ (Arrigo et al., 2011; Fransson et al., 2001; Kaltin et al., 2002; Land et al., 2013; Lauvset et al., 2013; Manizza et al., 2013, 2019; Omar et al., 2007; Takahashi et al., 2009; Yasunaka et al., 2016, 2018). Previous estimates of CO_2 uptake in the Chukchi Sea differ among the studies from 7.3 to $0.4 \text{ mol m}^{-2} \text{ yr}^{-1}$ (Bates, 2006; Evans et al., 2015; Kaltin & Anderson, 2005; Manizza et al., 2013, 2019; Murata & Takizawa, 2003; Takahashi et al., 2009; Yasunaka et al., 2016, 2018). The ensemble mean CO_2 uptake in the Chukchi Sea in the present study is $0.8 \pm 0.3 \text{ mol m}^{-2} \text{ yr}^{-1}$ in the $p\text{CO}_2$ products and $0.7 \pm 0.2 \text{ mol m}^{-2} \text{ yr}^{-1}$ in the models, which are near the lower limit of the previous estimates. In the atmospheric inversions, it is $0.1 \pm 0.3 \text{ mol m}^{-2} \text{ yr}^{-1}$. In the first implementation of RECCAP, the CO_2 uptake in the subregions was not assessed (Schuster et al., 2013).

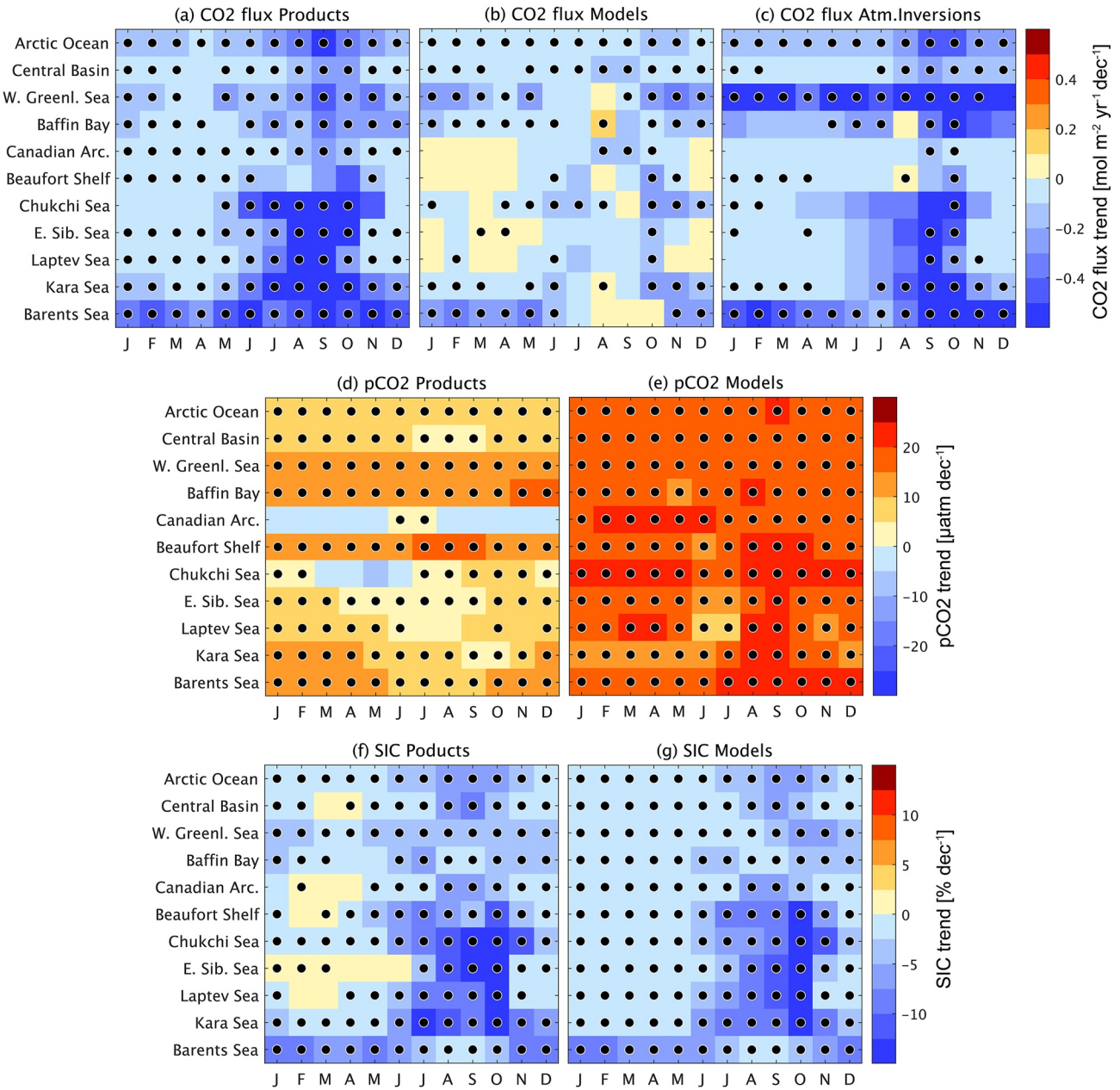


Figure 13. Trends in CO₂ flux, $p\text{CO}_{2w}$, and SIC over the 1985–2018 period from the $p\text{CO}_2$ products, the ocean biogeochemical hindcast and data assimilation models, and the atmospheric inversions. Negative values in panels (a) and (b) indicate increasing CO₂ influx to the ocean. Dots represent values in grids where more than two third of the estimates show the same sign of the trend. Ensemble means are calculated across the estimates, which cover the full period of 1985–2018 (see Table 1).

4.2. Uncertainty in Sea-Air CO₂ Flux and $p\text{CO}_{2w}$

4.2.1. Long-Term Mean

The CO₂ uptake in the Arctic Ocean is larger in the $p\text{CO}_2$ products ($116 \pm 4 \text{ TgC yr}^{-1}$) than in the ocean biogeochemical hindcast and data assimilation models ($92 \pm 30 \text{ TgC yr}^{-1}$). This difference might occur because most ocean models do not (fully) include the carbon input from land and the burial and remineralization in ocean sediments (Table 1; DeVries et al., 2023). According to Lacroix et al. (2020), this riverine-burial carbon flux was estimated to give rise to an outgassing of 29.7 TgC yr^{-1} in the Arctic Ocean, and it amplifies the difference between the $p\text{CO}_2$ product and the models, as this would need to be added to the flux in the $p\text{CO}_2$ products to make them comparable to the models, following procedures of, for example, the Global Carbon Budget (Friedlingstein

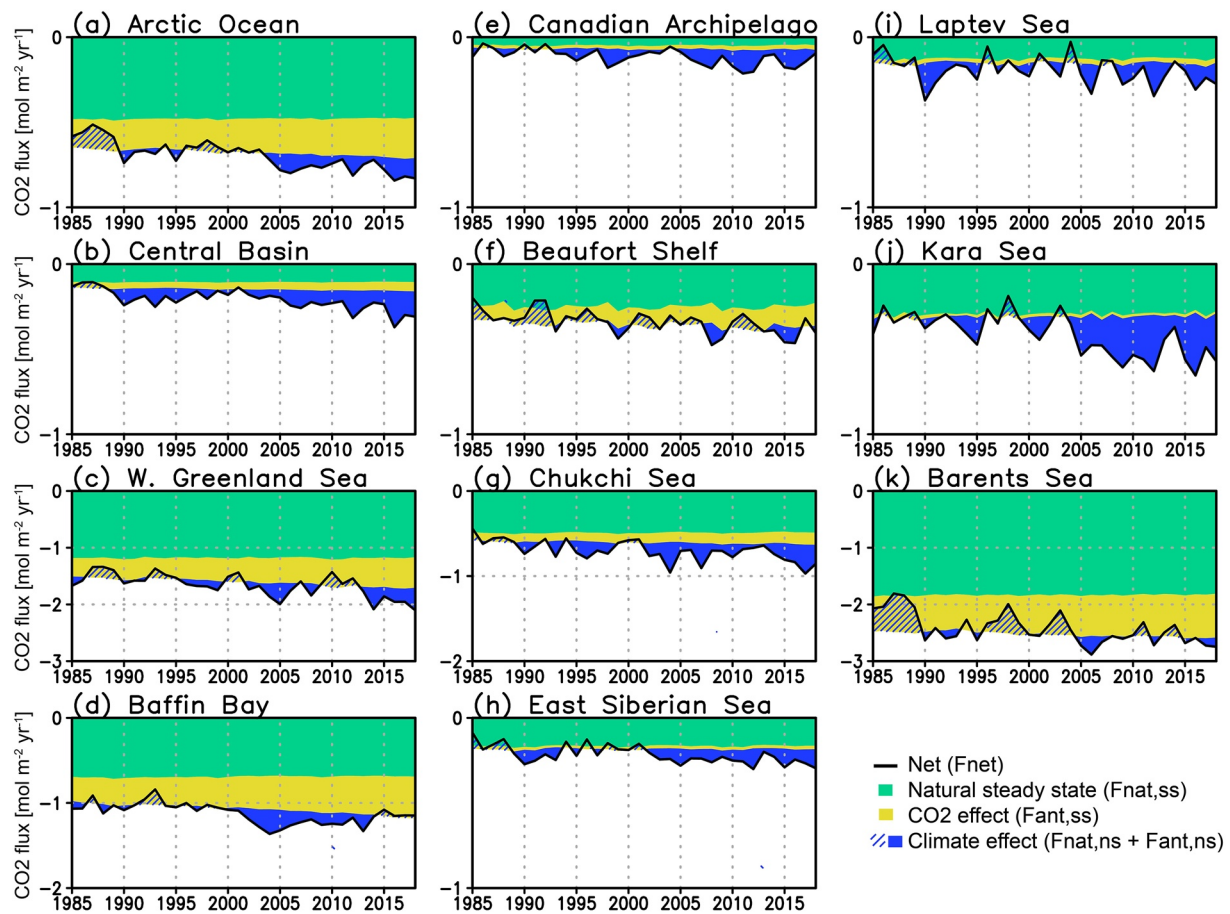


Figure 14. Time series of the decomposition of the net CO_2 flux (F_{net} ; black line) into the natural steady-state flux ($F_{\text{nat,ss}}$; aqua ribbon), the CO_2 effect ($F_{\text{ant,ss}}$; yellow ribbon), and the climate effect ($F_{\text{nat,ns}} + F_{\text{ant,ns}}$; blue hatch and ribbon). Negative values (or widths of the ribbons) indicate the CO_2 influx to the ocean, and positive values (or widths of the hatches) indicate CO_2 outflux from the ocean.

et al., 2022). However, the uncertainty of this adjustment is large because the ocean biogeochemical model used by Lacroix et al. (2020) does not resolve the Arctic Ocean small-scale dynamics due to the relatively coarse model resolution and likely does not capture the wide range of lability of organic carbon, sediment dynamics, or coastal erosion that are important for the carbon cycle in the Arctic Ocean (Brüchert et al., 2018; Couture et al., 2018; Freitas et al., 2020, 2021; Grotheer et al., 2020; Hilton et al., 2015; Holmes et al., 2008; Kaiser et al., 2017; Mann et al., 2012; Sanchez-Garcia et al., 2011; Vonk et al., 2012).

CAMS, which is one of the two inversions that covers the period 1985–2018, shows almost no flux in the Central Basin, the Canadian Archipelago, the Beaufort Shelf, the Chukchi Sea, the East Siberian Sea, the Laptev Sea and the Kara Sea even in summer (Figure 6; Figure S1 in Supporting Information S1) probably because the prior in these regions were set to be zero (Denvil-Sommer et al., 2019). The CO_2 flux in other atmospheric inversions might not differ a lot from the value determined by the oceanic prior because of the limited atmospheric CO_2 observations. Actually, the CO_2 flux in Jena-CarboScope is similar to that in Jena-MLS, which is used as a prior in Jena-CarboScope (Table S2; Figure S2 in Supporting Information S1).

4.2.2. Seasonal Cycle

The CO_2 uptake during summer and autumn in the Chukchi Sea, the Baffin Bay, the Kara Sea, and the Barents Sea is larger in the $p\text{CO}_2$ products than in the ocean biogeochemical hindcast and data assimilation models, which leads to the smaller annual uptake in the models there (Figures 6d, 6g, 6j, and 6k, respectively). The $p\text{CO}_{2w}$ from

the $p\text{CO}_2$ products is consistently lower than that from the models in these seasons and regions even though the observational data availability is different (Figures 7d, 7g, 7j, and 7k; Figure S1 in Supporting Information S1). The models do not reproduce the low $p\text{CO}_{2w}$ values observed in summer and the seasonal amplitudes of $p\text{CO}_{2w}$ are smaller in the models. Given that the seasonal SST amplitude in the models is similar to that in the products (Figure S8 in Supporting Information S1), the $p\text{CO}_{2w}$ differences cannot be explained by potentially different temperature effects on $p\text{CO}_{2w}$. Although differences in the biogeochemistry in the models may cause the discrepancy, there is insufficient observational data available to evaluate this. A similar discrepancy in the seasonal cycle of $p\text{CO}_{2w}$ between the products and the models has been found in the global ocean (Rogers et al., 2023).

Large discrepancies among the estimates of $p\text{CO}_{2w}$ are observed in the coastal parts of the East Siberian Sea, the Laptev Sea and the Kara Sea (Figure 7). A few ocean biogeochemical hindcast models (FESOM_REcoM_HR, FESOM_REcoM_LR, and Arctic_NEMURO-C) show high $p\text{CO}_{2w}$ values ($>500 \mu\text{atm}$) in winter in these regions (Figures 7h, 7i, and 7j), which leads to the annual CO_2 release in some cases (FESOM_REcoM_HR and FESOM_REcoM_LR; Table S2 in Supporting Information S1). Once the sea ice disappears in spring, the outgassing of CO_2 to the atmosphere (Figures 6h, 6i, and 6j) and intense phytoplankton blooms (not shown here) lower the $p\text{CO}_{2w}$ in those models. Remineralization below the surface or under sea ice of this newly formed organic matter then likely increases $p\text{CO}_{2w}$ values in winter. High $p\text{CO}_{2w}$ values ($>500 \mu\text{atm}$) were observed very near the coast in the Laptev Sea and the East Siberian Sea (Anderson et al., 2009), but the spatial and temporal extent of the high $p\text{CO}_{2w}$ has not yet been determined, and the $p\text{CO}_{2w}$ estimates in both the $p\text{CO}_2$ products and the models cannot be evaluated at this stage. Although general features of low SSS and low DIC in these regions due to fresh water input from rivers (Tank et al., 2012) are simulated in the models, the range of the model-simulated SSS and DIC are large (standard deviations are >2 in SSS and $>200 \mu\text{mol kg}^{-1}$ in DIC; not shown here) leading to inter-model differences in $p\text{CO}_{2w}$. This implies that the differences in the riverine water, carbon, alkalinity and nutrient input lead to large uncertainties in the $p\text{CO}_{2w}$ estimates in the ocean biogeochemical hindcast and data assimilation models. Other factors leading to large uncertainty in the coastal regions are burial, erosion and seafloor sediments, which are also difficult to evaluate at this stage. On the other hand, observations are scarce and biased towards summer and the open ocean, which may well lead to biases in the $p\text{CO}_2$ products based on $p\text{CO}_{2w}$ observations.

$p\text{CO}_{2w}$ in the Chukchi Sea is higher in the $p\text{CO}_2$ products than in the ocean biogeochemical hindcast and data assimilation models (Figure 7g). High $p\text{CO}_{2w}$ ($>500 \mu\text{atm}$) has sometimes been observed in the Chukchi Sea via storm-induced mixing events (Hauri et al., 2013), which may not be simulated in the models.

4.2.3. Trend From 1985 to 2018

The increasing trend in the CO_2 uptake is larger in the $p\text{CO}_2$ products and in the atmospheric inversions than in the ocean biogeochemical hindcast and data assimilation models in almost all regions and all seasons (Figures 9, 10a, 10b, and 13a–13c; Table S3 in Supporting Information S1). The decreasing trend in SIC is also larger in the $p\text{CO}_2$ products than in the models (Figures 10e, 10f, 13f, and 13g). Although the models reproduce SIC well not only in the mean distribution but also in the seasonal and interannual variability (Figures 4g, 8, 10f, 12, and 13f), small discrepancies in the SIC trends affect the trend in CO_2 flux (Figure S6 in Supporting Information S1). Furthermore, the increase in $p\text{CO}_{2w}$ is much larger in the models than in the $p\text{CO}_2$ product although the difference among the estimates is large (Figures 10c, 10d, 11, 13c, and 13d). Since the relevance of $p\text{CO}_{2w}$ for determining the CO_2 flux will increase along with the sea ice retreat over time, model improvement and more observations for the better $p\text{CO}_{2w}$ estimates are crucial.

The CO_2 uptake in the southern Barents Sea and the coastal region in the East Siberian Sea, the Laptev Sea, and the Kara Sea is increasing in the $p\text{CO}_2$ products but decreasing (or increasing outgassing in some regions that are CO_2 sources) in the ocean biogeochemical hindcast and data assimilation models (Figures 10a and 10b), but both estimates have large uncertainties in these regions as mentioned in Section 4.2.2. Recently, an increasing trend of summertime CO_2 uptake in the Chukchi Sea has been reported (Ouyang et al., 2020, 2022; Tu et al., 2021). In this study, the large increasing CO_2 uptake trend in the Chukchi Sea is detected in the $p\text{CO}_2$ products but it is small in the models (Figures 14a and 14b).

The trend in the global ocean CO_2 uptake is also larger in the $p\text{CO}_2$ products than in the ocean biogeochemical models ($380 \text{ TgC yr}^{-1} \text{ dec}^{-1}$ in the $p\text{CO}_2$ products $260 \text{ TgC yr}^{-1} \text{ dec}^{-1}$ in the ocean biogeochemical models from 2001 to 2018; DeVries et al., 2023). To resolve the temporal change of CO_2 uptake, more $p\text{CO}_2$ observations in

all seasons and implementing observed changes in riverine and coastal erosion fluxes, including the substantial temporal changes in the riverine alkalinity (Drake et al., 2018), into the ocean biogeochemical models (Behnke et al., 2021; Frey & McClelland, 2009; Peterson et al., 2002; Terhaar, Orr, Ethé, et al., 2019) are needed.

4.3. Importance of the Arctic Ocean CO₂ Flux for the Global Ocean Carbon Sink

Previous studies based on passive tracer observations have estimated that the Arctic Ocean anthropogenic carbon inventory (only due to increasing CO₂) by 2005 was 3.3 ± 0.3 Pg C (~2% of the change in the global ocean anthropogenic carbon inventory (scaled from Sabine et al. (2004), Tanhua et al. (2009), and Terhaar, Tanhua, et al. (2020)) although the Arctic Ocean volume represents only 1% of the global ocean volume (Jakobsson, 2002). Observations (Olsen et al., 2015) and model studies from hindcast models and Earth System Models (Terhaar, Orr, Gehlen, et al., 2019) suggest that one third of this anthropogenic carbon has been taken up in the Arctic Ocean and two thirds have been transported to the Arctic Ocean from the Atlantic and Pacific Oceans. Thus, the Arctic Ocean sea-air anthropogenic CO₂ flux accounts for less than 1% of the global ocean sea-air anthropogenic CO₂ flux. Actually, for the years from 1985 to 2018, we find that the anthropogenic sea-air CO₂ flux into the ocean to be 19 ± 6 Tg C yr⁻¹, ~1% of the global ocean anthropogenic sea-air CO₂ flux over the same period (DeVries et al., 2023). This relatively small contribution of the Arctic Ocean to the anthropogenic sea-air CO₂ flux may lead to the conclusion that the Arctic Ocean only plays a minor role in the global ocean carbon sink.

Our analysis, however, suggests that the importance of the Arctic Ocean for the global carbon sink has increased in the last decades. The anthropogenic sea-air CO₂ flux was augmented by an increasing uptake of natural carbon of 10 ± 17 TgC yr⁻¹ due to climate change (half of the anthropogenic sea-air CO₂ flux). The relatively large importance of the uptake of natural carbon suggests that observation-based estimates of the anthropogenic carbon storage in the Arctic Ocean underestimate the total change in DIC inventory and the associated historical acidification rates (Anderson et al., 2010; Tanhua et al., 2009; Terhaar, Tanhua, et al., 2020). Furthermore, the increase in the combined uptake of anthropogenic and natural carbon in the Arctic Ocean (31 ± 13 TgC yr⁻¹ dec⁻¹ in the *p*CO₂ products, 10 ± 5 TgC yr⁻¹ dec⁻¹ in the ocean biogeochemical hindcast and data assimilation models, and 5 TgC yr⁻¹ dec⁻¹ in the atmospheric inversion) is 4%–8% of the global ocean change in carbon uptake (380 TgC yr⁻¹ dec⁻¹ in the *p*CO₂ products and 260 TgC yr⁻¹ dec⁻¹ in the ocean biogeochemical models; DeVries et al., 2023). Thus, the Arctic Ocean contribution to the global ocean carbon sink remains relatively small but fast changes in the Arctic Ocean make it a relatively important ocean basin for changes in the estimated sea-air CO₂ flux. The Arctic Ocean's importance may further increase in the future when climate change and ocean warming are projected to cause further outgassing of natural carbon in most parts of the global ocean (Frölicher & Joos, 2010; Joos et al., 1999) and potentially further enhanced uptake of natural carbon in the Arctic Ocean (Frölicher & Joos, 2010).

5. Conclusions

We integrated results from the *p*CO₂ products based on surface ocean *p*CO_{2w} observation, ocean biogeochemical hindcast and data assimilation models and atmospheric inversions and presented synthesized estimates of the Arctic Ocean CO₂ uptake and their uncertainties. The Arctic Ocean is a net sink of CO₂ of 116 ± 4 TgC yr⁻¹ in the *p*CO₂ products, 92 ± 30 TgC yr⁻¹ in the models, and 92 ± 21 TgC yr⁻¹ in the atmospheric inversions. The CO₂ uptake peaks in late summer to early autumn and is low in winter because of the sea ice cover inhibiting sea-air fluxes. The annual mean of CO₂ uptake increased at a rate of 29 ± 11 TgC yr⁻¹ dec⁻¹ in the *p*CO₂ products, 10 ± 4 TgC yr⁻¹ dec⁻¹ in the models, and 32 ± 16 TgC yr⁻¹ dec⁻¹ in the atmospheric inversions.

The CO₂ uptake in the Arctic Ocean is primarily caused by steady-state fluxes of natural carbon ($70\% \pm 15\%$), and enhanced by the atmospheric CO₂ increase ($19\% \pm 5\%$) and climate change ($11\% \pm 18\%$). The Arctic Ocean is the only ocean where climate change influences the sea-air CO₂ flux by a similar magnitude as the increase in atmospheric CO₂. Moreover, the climate effect in the Arctic Ocean has become more important in recent years. The relatively strong importance of climate change is due to decreased sea ice cover that allows more CO₂ exchange via the sea-air interface.

The uncertainty remains large especially in the *p*CO_{2w} estimates in the East Siberian Sea and the Laptev Sea because of the limited observations in the *p*CO₂ products and limited or non-existing representation of carbon and nutrient coastal boundary fluxes from rivers, coastal erosion and sediment dynamics, and insufficient model

resolution to resolve small scale mixing in the models. Discrepancies in the seasonal cycle and long-term trend of $p\text{CO}_{2w}$ between the $p\text{CO}_2$ products and the ocean biogeochemical hindcast and data assimilation models were also observed in many other subregions of the Arctic Ocean. Furthermore, the true uncertainties may even be larger than the ensemble standard deviation due to common structural biases across the entire ensemble of estimates.

Further model development and more observations are crucially needed to improve estimates of the Arctic Ocean sea-air CO_2 fluxes in a time when the Arctic Ocean faces the effects of rapid change, such as SIC decrease, warming and increasing riverine inputs, that will ultimately also affect ecosystem drivers such as ocean acidification and changing net primary production (Terhaar, Kwiatkowski, & Bopp, 2020; Vancoppenolle et al., 2013).

Conflict of Interest

The authors declare no conflicts of interest relevant to this study.

Data Availability Statement

All sea-air CO_2 flux and $p\text{CO}_{2w}$ estimates in the RECCAP2 compilation and those provided on a personal basis are made available by Müller (2023) at <https://zenodo.org/record/7990823>. CAMS v20r2 and Jena-CarboScope sEXToc-NEET2021 sea-air CO_2 flux estimates were downloaded from <https://www.ecmwf.int/en/forecasts/dataset/cams-greenhouse-gas-ghg-flux-inversions> and <https://www.bgc-jena.mpg.de/CarboScope/>, respectively. Hadley Centre Sea Ice and SST data set, NOAA/National Snow and Ice Data Center Climate Data Record of Passive Microwave Sea Ice Concentration version 2, and NOAA Optimum Interpolation SST Version 2 were downloaded from the web sites (<https://www.metoffice.gov.uk/hadobs/hadisst/>; <http://nsidc.org/data/G02202/>; <http://www.esrl.noaa.gov/psd/data/gridded/data.noaa.oisst.v2.html>). SOCAT version 6 and LDEOv2017 are available on their web site (<http://www.socat.info/>; https://www.ncei.noaa.gov/access/ocean-carbon-acidification-data-system/oceans/LDEO_Underway_Data-base/). The NOAA Greenhouse Gas Marine Boundary Layer Reference product and sea-level pressure from NCEP2 were downloaded from the websites (<http://www.esrl.noaa.gov/gmd/ccgg/mb/index.html>; <http://www.esrl.noaa.gov/psd/data/gridded/data.ncep.reanalysis2.html>). The last access to the sites was on Oct 2, 2023.

References

- Anderson, L. G., Jutterström, S., Hjalmarsson, S., Wählström, I., & Semiletov, I. P. (2009). Out-gassing of CO_2 from Siberian Shelf seas by terrestrial organic matter decomposition. *Geophysical Research Letters*, 36(20), L20601. <https://doi.org/10.1029/2009GL040046>
- Anderson, L. G., & Kallin, S. (2001). Carbon fluxes in the Arctic Ocean-potential impact by climate change. *Polar Research*, 20(2), 225–232. <https://doi.org/10.3402/polar.v20i2.6521>
- Anderson, L. G., & Olsen, A. (2002). Air–sea flux of anthropogenic carbon dioxide in the North Atlantic. *Geophysical Research Letters*, 29(17), 16–21. <https://doi.org/10.1029/2002GL014820>
- Anderson, L. G., Tanhua, T., Björk, G., Hjalmarsson, S., Jones, E. P., Jutterström, S., et al. (2010). Arctic Ocean shelf–basin interaction: An active continental shelf CO_2 pump and its impact on the degree of calcium carbonate solubility. *Deep Sea Research Part I: Oceanographic Research Papers*, 57(7), 869–879. <https://doi.org/10.1016/j.dsr.2010.03.012>
- Arrigo, K., Pabi, S., van Dijken, G., & Maslowski, W. (2011). Air-sea flux of CO_2 in the Arctic Ocean, 1998–2003. *Journal of Geophysical Research*, 115(G4), G04024. <https://doi.org/10.1029/2009JG001224>
- Arrigo, K. R., & van Dijken, G. L. (2015). Continued increases in Arctic Ocean primary production. *Progress in Oceanography*, 136, 60–70. <https://doi.org/10.1016/j.pocean.2015.05.002>
- Årthun, M., Eldevik, T., Smedsrud, L. H., Skagseth, Ø., & Ingvaldsen, R. B. (2012). Quantifying the influence of Atlantic heat on Barents Sea ice variability and retreat. *Journal of Climate*, 25(13), 4736–4743. <https://doi.org/10.1175/JCLI-D-11-00466.1>
- Årthun, M., Onarheim, I. H., Dörr, J., & Eldevik, T. (2020). The seasonal and regional transition to an ice-free Arctic. *Geophysical Research Letters*, 48(1), e2020GL090825. <https://doi.org/10.1029/2020GL090825>
- Aumont, O., Ethé, C., Tagliabue, A., Bopp, L., & Gehlen, M. (2015). PISCES-v2: An ocean biogeochemical model for carbon and ecosystem studies. *Geoscientific Model Development*, 8, 2465–2513. <https://doi.org/10.5194/gmd-8-2465-2015>
- Bakker, D. C. E., Pfeil, B., Smith, K., Harasawa, S., Landa, C., Nakaoka, S., et al. (2016). A multi-decade record of high quality $f\text{CO}_2$ data in version 3 of the Surface Ocean CO_2 Atlas (SOCAT). *Earth System Science Data*, 8(2), 383–413. <https://doi.org/10.5194/essd-8-383-2016>
- Bates, N. R. (2006). Air-sea CO_2 fluxes and the continental shelf pump of carbon in the Chukchi Sea adjacent to the Arctic Ocean. *Journal of Geophysical Research*, 111(C10), C10013. <https://doi.org/10.1029/2005JC003083>
- Bates, N. R., Garley, R., Frey, K. E., Shake, K. L., & Mathis, J. T. (2014). Sea-ice melt CO_2 -carbonate chemistry in the western Arctic Ocean: Meltwater contributions to air-sea CO_2 gas exchange, mixed layer properties and rates of net community production under sea ice. *Biogeosciences*, 11(23), 6769–6789. <https://doi.org/10.5194/bg-11-6769-2014>
- Bates, N. R., & Mathis, J. T. (2009). The Arctic Ocean marine carbon cycle: Evaluation of air-sea CO_2 exchanges, ocean acidification impacts and potential feedbacks. *Biogeosciences*, 6(11), 2433–2459. <https://doi.org/10.5194/bg-6-2433-2009>
- Bates, N. R., Moran, S. B., Hansell, D. A., & Mathis, J. T. (2006). An increasing CO_2 sink in the Arctic Ocean due to sea-ice loss. *Geophysical Research Letters*, 33(23), L23609. <https://doi.org/10.1029/2006GL027028>

Acknowledgments

We thank the many researchers and funding agencies responsible for the product and model developments and the data submission to the RECCAP2 compilation, and for the collection of data and quality control for their contributions to SOCAT. This work was financially supported by the Arctic Challenge for Sustainability II (ArCS II) project funded by the Ministry of Education, Culture, Sports, Science and Technology, Japan, and JSPS KAKENHI Grant JP 20K04073. MF acknowledges the financial support from National Aeronautics and Space Agency through the Grant IDS19-0113. JT, PL, and JDM acknowledge support from the European Union's Horizon 2020 research and innovation programme under Grant agreement no. 821003 (project 4C). JT also acknowledges funding from the Woods Hole Oceanographic Institution Postdoctoral Scholar Program, and the Swiss National Science Foundation under Grant 200020_200511. AO appreciates funding from the Research Council of Norway (Grant 296012, N-ICOS-2). JH received funding from the Initiative and Networking Fund of the Helmholtz Association (Helmholtz Young Investigator Group Marine Carbon and Ecosystem Feedbacks in the Earth System (MarE-Sys), Grant VH-NG-1301).

- Behnke, M. I., McClelland, J. W., Tank, S. E., Kellerman, A. M., Holmes, R. M., Haghpour, N., et al. (2021). Pan-Arctic riverine dissolved organic matter: Synchronous molecular stability, shifting sources and subsidies. *Global Biogeochemical Cycles*, 35(4), e2020GB006871. <https://doi.org/10.1029/2020GB006871>
- Brüchert, V., Bröder, L., Sawicka, J. E., Tesi, T., Joye, S. P., Sun, X., et al. (2018). Carbon mineralization in Laptev and East Siberian sea shelf and slope sediment. *Biogeosciences*, 15(2), 471–490. <https://doi.org/10.5194/bg-15-471-2018>
- Cai, W. J., Chen, L. Q., Chen, B. S., Gao, Z. Y., Lee, S. H., Chen, J. F., et al. (2010). Decrease in the CO₂ uptake capacity in an ice-free Arctic Ocean Basin. *Science*, 329(5991), 556–559. <https://doi.org/10.1126/science.1189338>
- Carroll, D., Menemenlis, D., Adkins, J. F., Bowman, K. W., Brix, H., Dutkiewicz, S., et al. (2020). The ECCO-Darwin data-assimilative global ocean biogeochemistry model: Estimates of seasonal to multidecadal Surface Ocean pCO₂ and air-sea CO₂ flux. *Journal of Advances in Modeling Earth Systems*, 12(10), e2019MS001888. <https://doi.org/10.1029/2019MS001888>
- Chassignet, E. P., Yeager, S. G., Fox-Kemper, B., Bozec, A., Castruccio, F., Danabasoglu, G., et al. (2020). Impact of horizontal resolution on global ocean–sea ice model simulations based on the experimental protocols of the Ocean Model Intercomparison Project phase 2 (OMIP-2). *Geoscientific Model Development*, 13(9), 4595–4637. <https://doi.org/10.5194/gmd-13-4595-2020>
- Chau, T. T. T., Gehlen, M., & Chevallier, F. (2022). A seamless ensemble-based reconstruction of surface ocean pCO₂ and air–sea CO₂ fluxes over the global coastal and open oceans. *Biogeosciences*, 19(4), 1087–1109. <https://doi.org/10.5194/bg-19-1087-2022>
- Chevallier, F. (2020). Validation report for the CO₂ fluxes estimated by atmospheric inversion, v20r2. Retrieved from https://atmosphere.copernicus.eu/sites/default/files/custom-uploads/EQC-GHG/CAMS73_2018SC2_D73.1.4.1-2020-v5_202109_v1.pdf
- Chierici, M., Fransson, A., Lansard, B., Miller, L. A., Mucci, A., Shadwick, E., et al. (2011). The impact of biogeochemical processes and environmental factors on the calcium carbonate saturation state in the Circumpolar Flaw Lead in the Amundsen Gulf, Arctic Ocean. *Journal of Geophysical Research*, 116, C00G09. <https://doi.org/10.1029/2011JC007184>
- Comiso, J. C., Parkinson, C. L., Gersten, R., & Stock, L. (2008). Accelerated decline in the Arctic sea ice cover. *Geophysical Research Letters*, 35(1), L01703. <https://doi.org/10.1029/2007GL031972>
- Conway, T. J., Tans, P. P., Waterman, L. S., Thoning, K. W., Kitzis, D. R., Masarie, K. A., & Zhang, N. (1994). Evidence for interannual variability of the carbon cycle from the NOAA/CMDL global air sampling network. *Journal of Geophysical Research*, 99(D11), 22831–22855. <https://doi.org/10.1029/94jd01951>
- Couture, N. J., Irrgang, A., Pollard, W., Lantuit, H., & Fritz, M. (2018). Coastal erosion of permafrost soils along the Yukon Coastal Plain and fluxes of organic carbon to the Canadian Beaufort Sea. *Journal of Geophysical Research: Biogeosciences*, 123(2), 406–422. <https://doi.org/10.1002/2017JG004166>
- Denvil-Sommer, A., Gehlen, M., Vrac, M., & Mejia, C. (2019). LSCE-FFNN-v1: A two-step neural network model for the reconstruction of surface ocean pCO₂ over the global ocean. *Geoscientific Model Development*, 12(5), 2091–2105. <https://doi.org/10.5194/gmd-12-2091-2019>
- DeVries, T. (2014). The oceanic anthropogenic CO₂ sink: Storage, air-sea fluxes, and transports over the industrial era. *Global Biogeochemical Cycles*, 28(7), 631–647. <https://doi.org/10.1002/2013GB004739>
- DeVries, T. (2022). Atmospheric CO₂ and sea surface temperature variability cannot explain recent decadal variability of the ocean CO₂ sink. *Geophysical Research Letters*, 49(7), e2021GL096018. <https://doi.org/10.1029/2021GL096018>
- DeVries, T., Yamamoto, K., Wanninkhof, R., Gruber, N., Hauck, J., Müller, J. D., et al. (2023). Magnitude, trends, and variability of the global ocean carbon sink from 1985–2018. *Global Biogeochemical Cycles*, 37(10), in press. <https://doi.org/10.1029/2023GB007780>
- Doney, S. C., Lima, I., Feely, R. A., Glover, D. M., Lindsay, K., Mahowald, N., & Wanninkhof, J. K. M. R. (2009). Mechanisms governing interannual variability in upper-ocean inorganic carbon system and air-sea CO₂ fluxes: Physical climate and atmospheric dust. *Deep Sea Research Part II: Topical Studies in Oceanography*, 56(8–10), 640–655. <https://doi.org/10.1016/j.dsr2.2008.12.006>
- Döscher, R., Acosta, M., Alessandri, A., Anthoni, P., Arsouze, T., Bergman, T., et al. (2022). The EC-Earth3 Earth system model for the Coupled Model Intercomparison Project 6. *Geoscientific Model Development*, 15(7), 2973–3020. <https://doi.org/10.5194/gmd-15-2973-2022>
- Drake, T. W., Tank, S. E., Zhulidov, A. V., Holmes, R. M., Gurtovaya, T., & Spencer, R. G. (2018). Increasing alkalinity export from large Russian Arctic rivers. *Environmental Science & Technology*, 52(15), 8302–8308. <https://doi.org/10.1021/acs.est.8b01051>
- Else, B. G. T., Galley, R. J., Lansard, B., Barber, D. G., Brown, K., Miller, L., et al. (2013). Further observations of a decreasing atmospheric CO₂ uptake capacity in the Canada Basin (Arctic Ocean) due to sea ice loss. *Geophysical Research Letters*, 40(6), 1132–1137. <https://doi.org/10.1002/grl.50268>
- Evans, W., Mathis, J. T., Cross, J. N., Bates, N. R., Frey, K. E., Else, B. G. T., et al. (2015). Sea-air CO₂ exchange in the western Arctic coastal ocean. *Global Biogeochemical Cycles*, 29(8), 1190–1209. <https://doi.org/10.1002/2015GB005153>
- Fay, A. R., & McKinley, G. A. (2014). Global open-ocean biomes: Mean and temporal variability. *Earth System Science Data*, 6(2), 273–284. <https://doi.org/10.5194/essd-6-273-2014>
- Feng, L., Palmer, P. I., Parker, R. J., Deutscher, N. M., Feist, D. G., Kivi, R., et al. (2016). Estimates of European uptake of CO₂ inferred from GOSAT X CO₂ retrievals: Sensitivity to measurement bias inside and outside Europe. *Atmospheric Chemistry and Physics*, 16(3), 1289–1302. <https://doi.org/10.5194/acp-16-1289-2016>
- Fransson, A., Chierici, M., Anderson, L. G., Bussmann, I., Kattner, G., Peter Jones, E., & Swift, J. H. (2001). The importance of shelf processes for the modification of chemical constituents in the waters of the Eurasian Arctic Ocean: Implication for carbon fluxes. *Continental Shelf Research*, 21(3), 225–242. [https://doi.org/10.1016/S0278-4343\(00\)00088-1](https://doi.org/10.1016/S0278-4343(00)00088-1)
- Fransson, A., Chierici, M., Skjelvan, I., Olsen, A., Assmy, P., Peterson, A. K., et al. (2017). Effects of sea-ice and biogeochemical processes and storms on under-ice water fCO₂ during the winter-spring transition in the high Arctic Ocean: Implications for sea-air CO₂ fluxes. *Journal of Geophysical Research: Oceans*, 122(7), 5566–5587. <https://doi.org/10.1002/2016JC012478>
- Freitas, F. S., Hendry, K. R., Henley, S. F., Faust, J. C., Tessin, A. C., Stevenson, M. A., et al. (2020). Benthic-pelagic coupling in the Barents Sea: An integrated data-model framework. *Philosophical Transactions of the Royal Society A*, 378(2181), 20190359. <https://doi.org/10.1098/rsta.2019.0359>
- Freitas, F. S., Pika, P. A., Kasten, S., Jørgensen, B. B., Rassmann, J., Rabouille, C., et al. (2021). New insights into large-scale trends of apparent organic matter reactivity in marine sediments and patterns of benthic carbon transformation. *Biogeosciences*, 18(15), 4651–4679. <https://doi.org/10.5194/bg-18-4651-2021>
- Frey, K. E., & McClelland, J. W. (2009). Impacts of permafrost degradation on arctic river biogeochemistry. *Hydrological Processes*, 23(1), 169–182. <https://doi.org/10.1002/hyp.7196>
- Friedlingstein, P., Jones, M. W., O'Sullivan, M., Andrew, R. M., Bakker, D. C., Hauck, J., et al. (2022). Global carbon budget 2021. *Earth System Science Data*, 14(4), 1917–2005. <https://doi.org/10.5194/essd-14-1917-2022>
- Frölicher, T. L., & Joos, F. (2010). Reversible and irreversible impacts of greenhouse gas emissions in multi-century projections with the NCAR global coupled carbon cycle-climate model. *Climate Dynamics*, 35(7–8), 1439–1459. <https://doi.org/10.1007/s00382-009-0727-0>

- Gao, Z., Chen, L., Sun, H., Chen, B., & Cai, W.-J. (2012). Distributions and air–sea fluxes of carbon dioxide in the western Arctic Ocean. *Deep Sea Research Part II: Topical Studies in Oceanography*, 81–84, 46–52. <https://doi.org/10.1016/j.dsr2.2012.08.021>
- Gregor, L., & Gruber, N. (2021). OceanSODA-ETHZ: A global gridded data set of the surface ocean carbonate system for seasonal to decadal studies of ocean acidification. *Earth System Science Data*, 13(2), 777–808. <https://doi.org/10.5194/essd-13-777-2021>
- Grotheer, H., Meyer, V., Riedel, T., Pfalz, G., Mathieu, L., Hefter, J., et al. (2020). Burial and origin of permafrost-derived carbon in the nearshore zone of the southern Canadian Beaufort Sea. *Geophysical Research Letters*, 47(3), e2019GL085897. <https://doi.org/10.1029/2019GL085897>
- Hauck, J., Gregor, L., Nissen, C., Patara, L., Hague, M., Mongwe, P., et al. (2023). The Southern Ocean carbon cycle 1985–2018: Mean, seasonal cycle, trends and storage. *ESS Open Archive*. <https://doi.org/10.1029/2023GB007848>
- Hauck, J., Zeising, M., Le Quéré, C., Gruber, N., Bakker, D. C. E., Bopp, L., et al. (2020). Consistency and challenges in the ocean carbon sink estimate for the global carbon budget. *Frontiers in Marine Science*, 7, 571720. <https://doi.org/10.3389/fmars.2020.571720>
- Hauri, C., Winsor, P., Juranek, L. W., McDonnell, A. M., Takahashi, T., & Mathis, J. T. (2013). Wind-driven mixing causes a reduction in the strength of the continental shelf carbon pump in the Chukchi Sea. *Geophysical Research Letters*, 40(22), 5932–5936. <https://doi.org/10.1002/2013GL058267>
- Hersbach, H., Bell, B., Berrisford, P., Hirahara, S., Horányi, A., Muñoz-Sabater, J., et al. (2020). The ERA5 global reanalysis. *Quarterly Journal of the Royal Meteorological Society*, 146(730), 1999–2049. <https://doi.org/10.1002/qj.3803>
- Hilton, R. G., Galy, V., Gaillardet, J., Dellinger, M., Bryant, C., O'Regan, M., et al. (2015). Erosion of organic carbon in the Arctic as a geological carbon dioxide sink. *Nature*, 524(7563), 84–87. <https://doi.org/10.1038/nature14653>
- Holmes, R. M., McClelland, J. W., Raymond, P. A., Frazer, B. B., Peterson, B. J., & Stieglitz, M. (2008). Lability of DOC transported by Alaskan rivers to the Arctic Ocean. *Geophysical Research Letters*, 35(3), L03402. <https://doi.org/10.1029/2007GL032837>
- Jakobsson, M. (2002). Hypsometry and volume of the Arctic Ocean and its constituent seas. *Geochemistry, Geophysics, Geosystems*, 3(5), 1–18. <https://doi.org/10.1029/2001GC000302>
- Joos, F., Plattner, G. K., Stocker, T. F., Marchal, O., & Schmittner, A. (1999). Global warming and marine carbon cycle feedbacks on future atmospheric CO₂. *Science*, 284(5413), 464–467. <https://doi.org/10.1126/science.284.5413.464>
- Kaiser, K., Benner, R., & Amon, R. M. W. (2017). The fate of terrigenous dissolved organic carbon on the Eurasian shelves and export to the North Atlantic. *Journal of Geophysical Research: Oceans*, 122(1), 4–22. <https://doi.org/10.1002/2016JC012380>
- Kaltin, S., & Anderson, L. G. (2005). Uptake of atmospheric carbon dioxide in Arctic shelf seas: Evaluation of the relative importance of processes that influence pCO₂ in water transported over the Bering-Chukchi Sea shelf. *Marine Chemistry*, 94(1–4), 67–79. <https://doi.org/10.1016/j.marchem.2004.07.010>
- Kaltin, S., Anderson, L. G., Olsson, K., Fransson, A., & Chierici, M. (2002). Uptake of atmospheric carbon dioxide in the Barents Sea. *Journal of Marine Systems*, 38(1–2), 31–45. [https://doi.org/10.1016/S0924-7963\(02\)00168-9](https://doi.org/10.1016/S0924-7963(02)00168-9)
- Kanamitsu, M., Ebisuzaki, W., Woollen, J., Yang, S.-K., Hnilo, J. J., Fiorino, M., & Potter, G. L. (2002). NCEP-DOE AMIP-II reanalysis (R-2). *Bulletin of the American Meteorological Society*, 83(11), 1631–1643. <https://doi.org/10.1175/BAMS-83-11-1631>
- Kriest, I., & Oeschler, A. (2015). MOPS-1.0: Towards a model for the regulation of the global oceanic nitrogen budget by marine biogeochemical processes. *Geoscientific Model Development*, 8(9), 2929–2957. <https://doi.org/10.5194/gmd-8-2929-2015>
- Lacroix, F., Ilyina, T., & Hartmann, J. (2020). Oceanic CO₂ outgassing and biological production hotspots induced by pre-industrial river loads of nutrients and carbon in a global modeling approach. *Biogeosciences*, 17(1), 55–88. <https://doi.org/10.5194/bg-17-55-2020>
- Land, P. E., Shutler, J. D., Cowling, R. D., Woolf, D. K., Walker, P., Findlay, H. S., et al. (2013). Climate change impacts on sea-air fluxes of CO₂ in three Arctic seas: A sensitivity study using Earth observation. *Biogeosciences*, 10(12), 8109–8128. <https://doi.org/10.5194/bg-10-8109-2013>
- Landschützer, P., Laruelle, G. G., Roobaert, A., & Regnier, P. (2020). A uniform pCO₂ climatology combining open and coastal oceans. *Earth System Science Data*, 12(4), 2537–2553. <https://doi.org/10.5194/essd-12-2537-2020>
- Lauvset, S., Chierici, M., Counillon, F., Omar, A., Nondal, G., Johannessen, T., & Olsen, A. (2013). Annual and seasonal fCO₂ and air–sea CO₂ fluxes in the Barents Sea. *Journal of Marine Systems*, 113, 62–74. <https://doi.org/10.1016/j.jmarsys.2012.12.011>
- Levitus, S. (2013). *US DOC/NOAA/NESDIS > National Oceanographic Data Center. NODC standard product: World Ocean Atlas 2009 (NCEI Accession 0094866). Basin.msk*. NOAA National Centers for Environmental Information. Retrieved from <https://accession.nodc.noaa.gov/0094866>
- Liu, J., Baskaran, L., Bowman, K., Schimel, D., Bloom, A. A., Parazoo, N. C., et al. (2021). Carbon monitoring system flux net biosphere exchange 2020 (CMS-flux NBE 2020). *Earth System Science Data*, 13(2), 299–330. <https://doi.org/10.5194/essd-13-299-2021>
- Lundberg, L., & Haugan, P. M. (1996). A Nordic Seas–Arctic Ocean carbon budget from volume flows and inorganic carbon data. *Global Biogeochemical Cycles*, 10(3), 493–510. <https://doi.org/10.1029/96GB00359>
- MacGilchrist, G. A., Garabato, A. C. N., Tsubouchi, T., Bacon, S., Torres-Valdés, S., & Azetsu-Scott, K. (2014). The Arctic Ocean carbon sink. *Deep Sea Research Part I: Oceanographic Research Papers*, 86, 39–55. <https://doi.org/10.1016/j.dsr.2014.01.002>
- Manizza, M., Follows, M. J., Dutkiewicz, S., Menemenlis, D., Hill, C. N., & Key, R. M. (2013). Changes in the Arctic Ocean CO₂ sink (1996–2007): A regional model analysis. *Global Biogeochemical Cycles*, 27(4), 1108–1118. <https://doi.org/10.1002/2012GB004491>
- Manizza, M., Follows, M. J., Dutkiewicz, S., Menemenlis, D., McClelland, J. W., Hill, C. N., et al. (2011). A model of the Arctic Ocean carbon cycle. *Journal of Geophysical Research*, 116(C12), C12020. <https://doi.org/10.1029/2011JC006998>
- Manizza, M., Menemenlis, D., Zhang, H., & Miller, C. E. (2019). Modeling the recent changes in the Arctic Ocean CO₂ sink (2006–2013). *Global Biogeochemical Cycles*, 33(3), 420–438. <https://doi.org/10.1029/2018GB006070>
- Mann, P. J., Davydova, A., Zimov, N., Spencer, R. G. M., Davydov, S., Bulygina, E., et al. (2012). Controls on the composition and lability of dissolved organic matter in Siberia's Kolyma River basin. *Journal of Geophysical Research*, 117(G1), G01028. <https://doi.org/10.1029/2011JG001798>
- Mauritsen, T., Bader, J., Becker, T., Behrens, J., Bittner, M., Brokopf, R., et al. (2019). Developments in the MPI-M Earth System Model version 1.2 (MPI-ESM1.2) and its response to increasing CO₂. *Journal of Advances in Modeling Earth Systems*, 11(4), 998–1038. <https://doi.org/10.1029/2018MS001400>
- McGuire, A. D., Hayes, D. J., Kicklighter, D. W., Manizza, M., Zhuang, Q., Chen, M., et al. (2010). An analysis of the carbon balance of the Arctic Basin from 1997 to 2006. *Tellus B: Chemical and Physical Meteorology*, 62(5), 455–474. <https://doi.org/10.1111/j.1600-0889.2010.00497.x>
- Meier, W., Fetterer, F., Savoie, M., Mallory, S., Duerr, R., & Stroeve, J. (2013). *NOAA/NSIDC climate data record of passive microwave sea ice concentration. Version 2*. National Snow and Ice Data Center. <https://doi.org/10.7265/N55M63M1>
- Meredith, M., Sommerkorn, M., Cassotta, S., Derksen, C., Ekaykin, A., Hollowed, A., et al. (2019). Polar regions. In H.-O. Pörtner, D. C. Roberts, V. Masson-Delmotte, P. Zhai, M. Tignor, E. Poloczanska, et al. (Eds.), *IPCC special report on the ocean and cryosphere in a changing climate* (pp. 203–320). Cambridge University Press. <https://doi.org/10.1017/9781009157964.005>
- Müller, J. D. (2023). RECCAP2-ocean data collection [Dataset]. Zenodo. <https://doi.org/10.5281/zenodo.7990823>

- Murata, A., & Takizawa, T. (2003). Summertime CO₂ sink in shelf and slope waters of the western Arctic Ocean. *Continental Shelf Research*, 23(8), 753–776. [https://doi.org/10.1016/S0278-4343\(03\)00046-3](https://doi.org/10.1016/S0278-4343(03)00046-3)
- Nielsen, D. M., Pieper, P., Barkhordarian, A., Overduin, P., Ilyina, T., Brovkin, V., et al. (2022). Increase in Arctic coastal erosion and its sensitivity to warming in the twenty-first century. *Nature Climate Change*, 12(3), 263–270. <https://doi.org/10.1038/s41558-022-01281-0>
- Niwa, Y., Fujii, Y., Sawa, Y., Iida, Y., Ito, A., Satoh, M., et al. (2017). A 4D-Var inversion system based on the icosahedral grid model (NICAM-TM 4D-Var v1.0)—Part 2: Optimization scheme and identical twin experiment of atmospheric CO₂ inversion. *Geoscientific Model Development*, 10(6), 2201–2219. <https://doi.org/10.5194/gmd-10-2201-2017>
- Notz, D., & Stroeve, J. (2016). Observed Arctic sea-ice loss directly follows anthropogenic CO₂ emission. *Science*, 354(6313), 747–750. <https://doi.org/10.1126/science.aag2345>
- Olsen, A., Anderson, L. G., & Heinze, C. (2015). Arctic carbon cycle: Patterns, impacts and possible changes. *The New Arctic*, 95–115. https://doi.org/10.1007/978-3-319-17602-4_8
- Omar, A. M., Johannessen, T., Olsen, A., Kaitin, S., & Rey, F. (2007). Seasonal and interannual variability of the air-sea CO₂ flux in the Atlantic sector of the Barents Sea. *Marine Chemistry*, 104(3–4), 203–213. <https://doi.org/10.1016/j.marchem.2006.11.002>
- Onarheim, I. H., Eldevik, T., Smedsrud, L. H., & Stroeve, J. C. (2018). Seasonal and regional manifestation of Arctic sea ice loss. *Journal of Climate*, 31(12), 4917–4932. <https://doi.org/10.1175/JCLI-D-17-0427.1>
- Orr, J. C., Kwiatkowski, L., & Pörtner, H. O. (2022). Arctic Ocean annual high in pCO₂ could shift from winter to summer. *Nature*, 610(7930), 94–100. <https://doi.org/10.1038/s41586-022-05205-y>
- Ouyang, Z., Collins, A., Li, Y., Qi, D., Arrigo, K. R., Zhuang, Y., et al. (2022). Seasonal water mass evolution and non-redfield dynamics enhance CO₂ uptake in the Chukchi Sea. *Journal of Geophysical Research: Oceans*, 127(8), e2021JC018326. <https://doi.org/10.1029/2021JC018326>
- Ouyang, Z., Qi, D., Chen, L., Takahashi, T., Zhong, W., DeGrandpre, M. D., et al. (2020). Sea-ice loss amplifies summertime decadal CO₂ increase in the western Arctic Ocean. *Nature Climate Change*, 10(7), 678–684. <https://doi.org/10.1038/s41558-020-0784-2>
- Oziel, L., Baudena, A., Ardyna, M., Massicotte, P., Randelhoff, A., Sallée, J. B., et al. (2020). Faster Atlantic currents drive poleward expansion of temperate phytoplankton in the Arctic Ocean. *Nature Communications*, 11(1), 1–8. <https://doi.org/10.1038/s41467-020-15485-5>
- Oziel, L., Schourup-Kristensen, V., Wekerle, C., & Hauck, J. (2022). The pan-Arctic continental slope as an intensifying conveyor belt for nutrients in the central Arctic Ocean (1985–2015). *Global Biogeochemical Cycles*, 36(6), e2021GB007268. <https://doi.org/10.1029/2021GB007268>
- Peterson, B. J., Holmes, R. M., McClelland, J. W., Vorosmarty, C. J., Lammers, R. B., Shiklomanov, A. I., et al. (2002). Increasing river discharge to the Arctic Ocean. *Science*, 298(5601), 2171–2173. <https://doi.org/10.1126/science.1077445>
- Pierrot, D., Neill, C., Sullivan, K., Castle, R., Wanninkhof, R., Luger, H., et al. (2009). Recommendations for autonomous underway pCO₂ measuring systems and data-reduction routines. *Deep Sea Research Part II: Topical Studies in Oceanography*, 56(8–10), 512–522. <https://doi.org/10.1016/j.dsr2.2008.12.005>
- Qi, D., Ouyang, Z., Chen, L., Wu, Y., Lei, R., Chen, B., et al. (2022). Climate change drives rapid decadal acidification in the Arctic Ocean from 1994 to 2020. *Science*, 377(6614), 1544–1550. <https://doi.org/10.1126/science.abo0383>
- Rantanen, M., Karpechko, A. Y., Lipponen, A., Nordling, K., Hyvärinen, O., Ruosteenoja, K., et al. (2022). The Arctic has warmed nearly four times faster than the globe since 1979. *Communications Earth Environment*, 3(1), 1–10. <https://doi.org/10.1038/s43247-022-00498-3>
- Rayner, N. A. A., Parker, D. E., Horton, E. B., Folland, C. K., Alexander, L. V., Rowell, D. P., et al. (2003). Global analyses of sea surface temperature, sea ice, and night marine air temperature since the late nineteenth century. *Journal of Geophysical Research*, 108(D14), 4407. <https://doi.org/10.1029/2002JD002670>
- Reynolds, R. W., Rayner, N. A., Smith, T. M., Stokes, D. C., & Wang, W. (2002). An improved in situ and satellite SST analysis for climate. *Journal of Climate*, 15(13), 1609–1625. [https://doi.org/10.1175/1520-0442\(2002\)015<1609:AIISAS>2.0.CO;2](https://doi.org/10.1175/1520-0442(2002)015<1609:AIISAS>2.0.CO;2)
- Rödenbeck, C., DeVries, T., Hauck, J., Le Quéré, C., & Keeling, R. F. (2022). Data-based estimates of interannual sea-air CO₂ flux variations 1957–2020 and their relation to environmental drivers. *Biogeosciences*, 19(10), 2627–2652. <https://doi.org/10.5194/bg-19-2627-2022>
- Rödenbeck, C., Zaehle, S., Keeling, R., & Heimann, M. (2018). History of El Niño impacts on the global carbon cycle 1957–2017: A quantification from atmospheric CO₂ data. *Philosophical Transactions of the Royal Society B: Biological Sciences*, 373(1760), 20170303. <https://doi.org/10.1098/rstb.2017.0303>
- Rodgers, K. B., Schwinger, J., Fassbender, A. J., Landschützer, P., Yamaguchi, R., Frenzel, H., et al. (2023). Seasonal variability of the surface ocean carbon cycle: A synthesis. *Global Biogeochemical Cycles*, 37(9), e2023GB007798. <https://doi.org/10.1029/2023gb007798>
- Sabine, C. L., Feely, R. A., Gruber, N., Key, R. M., Lee, K., Bullister, J. L., et al. (2004). The oceanic sink for anthropogenic CO₂. *Science*, 305(5682), 367–371. <https://doi.org/10.1126/science.1097403>
- Sánchez-García, L., Alling, V., Pugach, S., Vonk, J., Van Dongen, B., Humborg, C., et al. (2011). Inventories and behavior of particulate organic carbon in the Laptev and East Siberian seas. *Global Biogeochemical Cycles*, 25(2). <https://doi.org/10.1029/2010GB003862>
- Schmidt, S., Johnson, G. C., & Lyman, J. M. (2013). MIMOC: A global monthly isopycnal upper-ocean climatology with mixed layers. *Journal of Geophysical Research: Oceans*, 118(4), 1658–1672. <https://doi.org/10.1002/jgrc.20122>
- Schuster, U., McKinley, G. A., Bates, N., Chevallier, F., Doney, S. C., Fay, A. R., et al. (2013). An assessment of the Atlantic and Arctic sea-air CO₂ fluxes. *Biogeosciences*, 10(1), 607–627. <https://doi.org/10.5194/bg-10-607-2013>
- Schwinger, J., Goris, N., Tjiputra, J. F., Kriest, I., Bentsen, M., Bethke, I., et al. (2016). Evaluation of NorESM-OC (versions 1 and 1.2), the ocean carbon-cycle stand-alone configuration of the Norwegian Earth System Model (NorESM1). *Geoscientific Model Development*, 9(8), 2589–2622. <https://doi.org/10.5194/gmd-9-2589-2016>
- Screen, J., & Simmonds, I. (2010). The central role of diminishing sea ice in recent Arctic temperature amplification. *Nature*, 464(7293), 1334–1337. <https://doi.org/10.1038/nature09051>
- Séférian, R., Nabat, P., Michou, M., Saint-Martin, D., Voltaire, A., Colin, J., et al. (2019). Evaluation of CNRM Earth system model, CNRM-ESM2-1: Role of Earth system processes in present-day and future climate. *Journal of Advances in Modeling Earth Systems*, 11(12), 4182–4227. <https://doi.org/10.1029/2019MS001791>
- Stock, C. A., Dunne, J. P., Fan, S., Ginoux, P., John, J., Krasting, J. P., et al. (2020). Ocean biogeochemistry in GFDL's Earth system model 4.1 and its response to increasing atmospheric CO₂. *Journal of Advances in Modeling Earth Systems*, 12(10), e2019MS002043. <https://doi.org/10.1029/2019MS002043>
- Takahashi, T., Sutherland, S. C., & Kozyr, A. (2018). *Global ocean surface water partial pressure of CO₂ database: Measurements performed during 1957–2017 (LDEO database version 2017) (NCEI Accession 0160492) (version 4.4)*. LDEO_Database_V2017. NOAA National Centers for Environmental Information. [https://doi.org/10.3334/CDIAC/OTG.NDPO88\(V2015\)](https://doi.org/10.3334/CDIAC/OTG.NDPO88(V2015))
- Takahashi, T., Sutherland, S. C., Wanninkhof, R., Sweeney, C., Feely, R. A., Chipman, D. W., et al. (2009). Climatological mean and decadal change in surface ocean pCO₂ and net sea-air CO₂ flux over the global oceans. *Deep Sea Research Part II: Topical Studies in Oceanography*, 56(8–10), 554–577. <https://doi.org/10.1016/j.dsr2.2008.12.009>

- Tanhua, T., Jones, E. P., Jeansson, E., Jutterström, S., Smethie, W. M., Jr., Wallace, D. W., & Anderson, L. G. (2009). Ventilation of the Arctic Ocean: Mean ages and inventories of anthropogenic CO₂ and CFC-11. *Journal of Geophysical Research*, *114*(C1), C01002. <https://doi.org/10.1029/2008JC004868>
- Tank, S. E., Raymond, P. A., Striegl, R. G., McClelland, J. W., Holmes, R. M., Fiske, G. J., & Peterson, B. J. (2012). A land-to-ocean perspective on the magnitude, source and implication of DIC flux from major Arctic rivers to the Arctic Ocean. *Global Biogeochemical Cycles*, *26*(4), GB4018. <https://doi.org/10.1029/2011GB00041>
- Tank, S. E., Striegl, R. G., McClelland, J. W., & Kokelj, S. V. (2016). Multi-decadal increases in dissolved organic carbon and alkalinity flux from the Mackenzie drainage basin to the Arctic Ocean. *Environmental Research Letters*, *11*(5), 054015. <https://doi.org/10.1088/1748-9326/11/5/054015>
- Tanski, G., Bröder, L., Wagner, D., Knoblauch, C., Lantuit, H., Beer, C., et al. (2021). Permafrost carbon and CO₂ pathways differ at contrasting coastal erosion sites in the Canadian Arctic. *Frontiers in Earth Science*, *207*. <https://doi.org/10.3389/feart.2021.630493>
- Terhaar, J., Goris, N., Müller, J. D., DeVries, T., Gruber, N., Hauck, J., et al. (2023). Assessment of global ocean biogeochemistry models for ocean carbon sink estimates in RECCAP2 and recommendations for future studies. *ESS Open Archive*. <https://doi.org/10.22541/essoar.168394734.41886821/v1>
- Terhaar, J., Kwiatkowski, L., & Bopp, L. (2020). Emergent constraint on Arctic Ocean acidification in the twenty-first century. *Nature*, *582*(7812), 379–383. <https://doi.org/10.1038/s41586-020-2360-3>
- Terhaar, J., Orr, J. C., Ethé, C., Regnier, P., & Bopp, L. (2019). Simulated Arctic Ocean response to doubling of riverine carbon and nutrient delivery. *Global Biogeochemical Cycles*, *33*(8), 1048–1070. <https://doi.org/10.1029/2019GB006200>
- Terhaar, J., Orr, J. C., Gehlen, M., Ethé, C., & Bopp, L. (2019). Model constraints on the anthropogenic carbon budget of the Arctic Ocean. *Biogeosciences*, *16*(11), 2343–2367. <https://doi.org/10.5194/bg-16-2343-2019>
- Terhaar, J., Tanhua, T., Stöven, T., Orr, J. C., & Bopp, L. (2020). Evaluation of data-based estimates of anthropogenic carbon in the Arctic Ocean. *Journal of Geophysical Research: Oceans*, *125*(6), e2020JC016124. <https://doi.org/10.1029/2020JC016124>
- Tu, Z., Le, C., Bai, Y., Jiang, Z., Wu, Y., Ouyang, Z., et al. (2021). Increase in CO₂ uptake capacity in the Arctic Chukchi Sea during summer revealed by satellite-based estimation. *Geophysical Research Letters*, *48*(15), e2021GL093844. <https://doi.org/10.1029/2021GL0>
- Urakawa, L. S., Tsujino, H., Nakano, H., Sakamoto, K., Yamanaka, G., & Toyoda, T. (2020). The sensitivity of a depth-coordinate model to diapycnal mixing induced by practical implementations of the isopycnal tracer diffusion scheme. *Ocean Modelling*, *154*, 101693. <https://doi.org/10.1016/j.ocemod.2020.101693>
- Vancoppenolle, M., Bopp, L., Madec, G., Dunne, J., Ilyina, T., Halloran, P. R., & Steiner, N. (2013). Future Arctic Ocean primary productivity from CMIP5 simulations: Uncertain outcome, but consistent mechanisms. *Global Biogeochemical Cycles*, *27*(3), 605–619. <https://doi.org/10.1002/gbc.20055>
- Van Der Laan-Luijkx, I. T., Van Der Velde, I. R., Van Der Veen, E., Tsuruta, A., Stanislawski, K., Babenhausserheide, A., et al. (2017). The CarbonTracker Data Assimilation Shell (CTDAS) v1. 0: Implementation and global carbon balance 2001–2015. *Geoscientific Model Development*, *10*(7), 2785–2800. <https://doi.org/10.5194/gmd-10-2785-2017>
- Völker, C., Wallace, D. W., & Wolf-Gladrow, D. A. (2002). On the role of heat fluxes in the uptake of anthropogenic carbon in the North Atlantic. *Global Biogeochemical Cycles*, *16*(4), 85–91. <https://doi.org/10.1029/2002GB001897>
- Vonk, J. E., Sánchez-García, L., Van Dongen, B. E., Alling, V., Kosmach, D., Charkin, A., et al. (2012). Activation of old carbon by erosion of coastal and subsea permafrost in Arctic Siberia. *Nature*, *489*(7414), 137–140. <https://doi.org/10.1038/nature11392>
- Vowinkel, E., & Orvig, S. (1962). Water balance and heat flow of the Arctic Ocean. *Arctic*, *15*(3), 205–223. <https://doi.org/10.14430/arctic3574>
- Wang, Q., Wekerle, C., Wang, X., Danilov, S., Koldunov, N., Sein, D., et al. (2020). Intensification of the Atlantic water supply to the Arctic Ocean through Fram Strait induced by Arctic sea ice decline. *Geophysical Research Letters*, *57*(3), e2019GL086682. <https://doi.org/10.1029/2019GL086682>
- Watanabe, E., Jin, M., Hayashida, H., Zhang, J., & Steiner, N. (2019). Multi-model intercomparison of the pan-Arctic ice-algal productivity on seasonal, interannual, and decadal timescales. *Journal of Geophysical Research: Oceans*, *124*(12), 9053–9084. <https://doi.org/10.1029/2019JC015100>
- Weiss, R. F. (1974). Carbon dioxide in water and seawater: The solubility of a non-ideal gas. *Marine Chemistry*, *2*(3), 203–215. [https://doi.org/10.1016/0304-4203\(74\)90015-2](https://doi.org/10.1016/0304-4203(74)90015-2)
- Wright, R. M., Le Quéré, C., Buitenhuis, E., Pitois, S., & Gibbons, M. J. (2021). Role of jellyfish in the plankton ecosystem revealed using a global ocean biogeochemical model. *Biogeosciences*, *18*(4), 1291–1320. <https://doi.org/10.5194/bg-18-1291-2021>
- Yang, S., & Gruber, N. (2016). The anthropogenic perturbation of the marine nitrogen cycle by atmospheric deposition: Nitrogen cycle feedbacks and the 15N Haber-Bosch effect. *Global Biogeochemical Cycles*, *30*(10), 1418–1440. <https://doi.org/10.1002/2016GB005421>
- Yasunaka, S., Murata, A., Watanabe, E., Chierici, M., Fransson, A., van Heuven, S., et al. (2016). Mapping of the air–sea CO₂ flux in the Arctic Ocean and its adjacent seas: Basin-wide distribution and seasonal to interannual variability. *Polar Science*, *10*(3), 323–334. <https://doi.org/10.1016/j.polar.2016.03.006>
- Yasunaka, S., Siswanto, E., Olsen, A., Hoppema, M., Watanabe, E., Fransson, A., et al. (2018). Arctic Ocean CO₂ uptake: An improved multi-year estimate of the air–sea CO₂ flux incorporating chlorophyll a concentrations. *Biogeosciences*, *15*(6), 1643–1661. <https://doi.org/10.5194/bg-15-1643-2018>
- Zeng, J., Matsunaga, T., & Shirai, T. (2022). A new estimate of oceanic CO₂ fluxes by machine learning reveals the impact of CO₂ trends in different methods. *Earth System Science Data Discussions*.